The Relationships between Weight Functions, Geometric Functions, and Compliance Functions in Linear Elastic Fracture Mechanics

by

Rong Yuan

B.E. (Tsinghua University, Beijingg, China) 1999
M.S. (University of California, Berkeley) 2004

A dissertation submitted in partial satisfaction of the

requirements for the degree of

Doctor of Philosophy

in

Engineering-Materials Science and Engineering

in the

Graduate Division

of the

University of California, Berkeley

Committee in charge:

Professor Robert O. Ritchie, Chair
Professor Lutgard C. De Jonghe
Professor Panos Papadopoulos

Spring 2007

Abstract

The relationships between weight functions, geometric functions, and compliance functions in linear elastic fracture mechanics

by

Rong Yuan

Doctor of Philosophy in Engineering-Materials Science and Engineering

University of California, Berkeley

Professor R. O. Ritchie, Chair

Linear elastic fracture mechanics is widely used in industry because it established simple and explicit relationships between the permissible loading conditions and the critical crack size that is allowed in a structure. Stress intensity factors are the above-mentioned functional expressions that relate load with crack size through geometric functions or weight functions. Compliance functions are to determine the crack/flaw size in a structure when optical inspection is inconvenient. As a result, geometric functions, weight functions and compliance functions have been intensively studied to determine the stress intensity factor expressions for different geometries. However, the relations between these functions have received less attention. This work is therefore to investigate the intrinsic relationships between these functions.

Theoretical derivation was carried out and the results were verified on single-edge cracked plate under tension and bending. It is found out that the geometric function is essentially the non-dimensional weight function at the loading point. The compliance function is composed of two parts: a varying part due to crack extension and a constant

part from the intact structure if no crack exists. The derivative of the compliance function at any location is the product of the geometric function and the weight function at the evaluation point. Inversely, the compliance function can be acquired by the integration of the product of the geometric function and the weight function with respect to the crack size. The integral constant is just the unchanging compliance from the intact structure. Consequently, a special application of the relations is to obtain the compliance functions along a crack once the geometric function and weight functions are known. Any of the three special functions can be derived once the other two functions are known. These relations may greatly simplify the numerical process in obtaining either geometric functions, weight functions or compliance functions for new test geometries.

Professor Robert O. Ritchie
Dissertation Committee Chair

To

my parents, my husband Yun, and my dream

TABLE OF CONTENTS

List of Symbols ····· iv

List of Figures ····· ix

List of Tables ····· xi

Acknowledgements ····· xii

Chapter 1: Synopsis ····· 1

References ····· 2

Chapter 2: Background on Fracture Mechanics ····· 3

2.1 Scope and Definition ····· 3

2.2 Thermodynamics in Fracture Mechanics ····· 5

2.2.1 Some Terms in Thermodynamics ····· 5

2.2.1.1 State Functions and Transitional Quantities ····· 6

2.2.1.2 Quasi-Static vs. Reversible Transitions ····· 6

2.2.2 Energy Release Rate by the First Law ····· 6

2.2.2.1 Energy Release Rate and Fracture Criteria ····· 6

2.2.2.2 Meaning of the Energy Release Rate ····· 9

2.2.3 Historical Review on Energy Release Rate ····· 11

2.2.3.1 Griffith's Work in Elasticity ····· 11

2.2.3.2 Irwin's Modification for Plasticity ····· 14

2.2.3.3 J-integral Method ····· 16

2.3 Constitutive Laws ····· 18

2.3.1 Linear Elasticity ····· 18
2.3.2 Linear Elasticity-Perfect Plasticity ····· 19
2.3.2.1 Irwin's Solution ····· 19
2.3.2.2 Von Mises Yield Criterion ····· 21
2.3.3 Cohesive Zone Models ····· 21
2.3.3.1 Dugdale's Model: Linear Elasticity-Perfect Plasticity ····· 22
2.3.3.2 Barenblatt's Work ····· 22
2.4 Summary ····· 23
References ····· 24
Tables and Figures ····· 25
Chapter 3: The Relationships between Weight Functions, Geometric Functions, and Compliance Functions in Linear Elastic Fracture Mechanics ····· 33
3.1 Introduction ····· 33
3.2 Special Functions ····· 34
3.2.1 Geometric Function ····· 35
3.2.2 Weight Function ····· 36
3.2.3 Compliance Function ····· 37
3.3 Relationships between Weight Functions, Geometric Functions, and Compliance Functions ····· 38
3.3.1 Weight Function and Geometric Function ····· 38
3.3.2 Weight Function and Compliance Function ····· 38
3.3.3 Geometric Function and the Load-Point Compliance Function ····· 39
3.3.4 Discussion ····· 40

3.3.4.1 Integral Constants for Displacement Fields and Compliance Functions ····· 40
3.3.4.2 Comparison of the Special Functions ····· 40
3.4 An Example on Single-Edge Cracked Plate ····· 41
3.4.1 Uniform Tension ····· 41
3.4.2 CMOD Compliance for the 3-Point Bend Specimen ····· 42
3.5 Summary and Conclusions ····· 43
References ····· 44
Tables and Figures ····· 45
Chapter 4: Elastic Compliance Functions for the Notched Four-Point Bend Specimen 51
4.1 Introduction ····· 51
4.2 Experiments and Simulation ····· 53
4.2.1 Specimen Geometry and K_I Solutions ····· 53
4.2.2 Experimental Procedures ····· 54
4.2.3 Numerical Methods ····· 54
4.3 Results and Discussion ····· 55
4.3.1 Crack-Mouth Opening Displacement (CMOD) ····· 55
4.3.2 Back-Face Strain (BFS) Compliance ····· 56
4.3.3 Load-Point Displacement (LPD) ····· 56
4.4 Summary and Conclusions ····· 58
References ····· 58
Tables and Figures ····· 60
Chapter 5: Conclusions ····· 68

LIST OF SYMBOLS

Abbreviations and Subscripts

avg: average value

BCs: boundary conditions

BFS: back face strain

cm: crack mouth

CMOD: crack-mouth opening displacement

LEFM: linear elastic fracture mechanics

LPD: load-point displacement

$_A$: externally applied

lp, $_{lp}$: at load-point

$_{nc}$: intact structure if crack did not exist

$_P$: at constant loading

I, II, III: loading modes of tension, shear, and tear, respectively

Coordinates

(x, y, z) or (x_1, x_2, x_3) : Cartesian coordinates

r, θ : polar coordinates

i, j: indices denoting either Cartesian or polar coordinates

$\underset{\sim}{x}$: position on a cracked body

Body and Configuration

Ω: 2-D or 3-D cracked elastic body

$d\Omega$: infinitesimal area (or volume)

Γ: 1-D contour of the elastic body in a plane

l: length of the 1-D contour of an elastic body where stress is acted

Spatial Measures

a: crack length

A: crack area

B: thickness

d: minor span of a four-point bend specimen; or size of the plastic zone in Dugdale's model

r_P : size of the plastic zone in Irwin's model

r_Y : characteristic length where elastic stress reaches the yield strength

S: major span of a four-point bend specimen

W: width

α: normalized crack length, $\alpha = a / W$

ρ: atomic bond length

Deformation

ε: strain

u, u_{lp}: displacement

$u(\underset{\sim}{x})$, $u(\underset{\sim}{x}, a)$, $u(\underset{\sim}{x}, \alpha)$: displacement as a function of position $\underset{\sim}{x}$ or/and crack length a or normalized crack length α

$u_{nc}(\underset{\sim}{x})$: displacement of a loaded structure if crack did not exist; as a function of position $\underset{\sim}{x}$ only

$u(cm, \alpha)$: displacement at the crack mouth

Δ: total displacement

Loading

σ: stress

$\sigma_1, \sigma_2, \sigma_3$: principal stresses determined by Mohr's circle

σ_e : equivalent stress defined by von Mises yield criterion

σ_F : failure strength

σ_{th} : theoretical ultimate strength

σ_Y : yield strength under uniform tension

σ_A , t, $t(\underset{\sim}{x})$: far-field applied traction

$p(r)$: cohesive stress in Barenblatt's cohesive zone, as a function of the position in the zone

P: force

M: bending moment

Compliance and Modulus

C: compliance as a ratio of deformation to loading

$\tilde{C}(\underset{\sim}{x}, \alpha)$: non-dimensional compliance as a function of position $\underset{\sim}{x}$ and normalized crack length α

$\tilde{C}(lp, \alpha)$: non-dimensional compliance at loading point

$\tilde{C}(cm, \alpha)$: non-dimensional compliance at the crack mouth

$\tilde{C}_{nc}(\underset{\sim}{x})$: non-dimensional compliance of an structure if crack did not exist; as a function of position $\underset{\sim}{x}$ only

E: Young's modulus: E in plane stress condition; $E/(1-\nu^2)$ in plane strain condition

ν: Poisson's ratio

μ: shear modulus, and $\mu = \frac{E}{2(1+\nu)}$

Energy related terms

Q: heat

U: internal energy

w: strain energy density

$U_{strain}^{elastic}$: elastic strain energy

$U_{strain}^{plastic}$: plastic strain energy

U^* : complimentary strain energy

$\mathcal{V}$: virtual work at constant loading

$\mathcal{W}$: actual work done on the cracked body

Π: potential energy

Fracture-property related terms

$\mathcal{G}$: energy release rate or crack driving force

J: J-integral that has the same meaning as energy release rate

$\mathcal{R}$: fracture toughness

γ : surface energy

$\gamma^{plastic}$: plastic deformation per unit crack-area

K, $K(a)$, $K(\alpha)$: stress intensity factor, only meaningful in LEFM, as a function of crack length a or normalized crack length α

K_{eff} : effective stress intensity factor outside the plastic zone in Irwin's model for small scale yielding at the crack tip

Functional Relations

Ψ(θ), Θ(θ): angular distribution respectively of displacement and stress near crack tip as a non-dimensional function of θ

f(a/W), f(α), Q(α), Q*(α): geometric function as a non-dimensional function of normalized crack

$h(\underset{\sim}{x},a)$, $h(\underset{\sim}{x},\alpha)$: weight function as a function of position $\underset{\sim}{x}$ and crack length a or α

$\tilde{h}_I(\underset{\sim}{x},\alpha)$, $\tilde{h}(\underset{\sim}{x},\alpha)$,: non-dimensional weight function

$\tilde{h}(avg,\alpha)$: averaged non-dimensional weight function along 1-D boundary Γ where stress is acted

$\tilde{h}(cm,\alpha)$: non-dimensional weight function at the crack mouth

$\tilde{h}(lp,\alpha)$: non-dimensional weight function at load point

O($\sqrt{r}$) : higher-order terms of $\sqrt{r}$

Thermodynamic properties

T: temperature

S: entropy

LIST OF FIGURES

Fig. 2.1 Scheme of fracture mechanics as an interdisciplinary field of materials science and solid mechanics.

Fig. 2.2 A quasi-static crack propagation in a cracked elastic body from crack size a_1 (a) to a_2 (d) after a loading-unloading cycle (e). When the crack is about to propagate (b), the external work done on the system is balanced by the elastic strain energy (area A and B). After propagation, the external work is balanced by the elastic strain energy (area B and D) at the new crack length and the surface energy of the new crack (area A and C).

Fig. 2.3 A cracked 2-D elastic solid structure Ω, where Γ_0 is the boundary enclosing Ω except the crack surfaces, Γ_1 is an arbitrary path inside Ω, and Γ_2 is the elastic-plastic interface. The region enclosed by Γ_2 and the crack is the plastic deformation zone.

Fig. 2.4 Different constitutive behaviors of materials, where σ_Y is the yield strength determined from uniform tension test and ε_Y is the strain resulting from the yield strength.

Fig. 2.5 Irwin's elastoplastic stress solution at the crack tip under small scale yielding condition. The broken curve represents the stress solution at the crack tip in linear elasticity, and the solid curve is Irwin's stress solution at the crack tip for linear elastic-perfectly plastic material under small scale yielding condition.

Fig. 2.6 The plastic zone shape at the crack tip under Mode I by von Mises criterion. The crack tip is located at the origin. Crack is located along $-x$ axis. The plot shows the contour of the constant equivalent stress σ_e ($=\sigma_Y$) upon yielding respectively in plane stress and plane strain condition.

Fig. 2.7 Illustration of Dugdale's Model. A crack resides in a large steel sheet subject to far-field uniform tension. The length of the cohesive zone (a) is d, and the height of the cohesive zone (b) is the same as the thickness. The slip lines are 45 degrees to the x_2 and x_3 axes.

Fig. 3.1 Symmetric specimen under symmetric loading of either (a) concentrated forces or (b) traction along the boundary. The load-displacement curve shows that the actual work is the area OAB and the virtual work is area OABC in LEFM.

Fig. 3.2 Schematic plots of linear superposition of displacement field, stress field, and stress intensity factor in an elastic body with different crack length, subjected to a constant load. Obviously, the contribution of displacement, stress, and stress intensity factor are all constant if the external loading is constant during crack propagation.

Fig. 3.3 Scheme of single-edge cracked plate (a) loaded under far-field uniform tension (b) and under 3-pt bending (c).

Fig. 3.4 Plot of the non-dimensional weight function of single-edge cracked plate at the crack mouth as a function of normalized crack length α, showing the weight function derived from Eq. (3.12) employing the relation between the geometric function and the CMOD compliance function (solid circles), as compared to Fett's solution [5] (solid line).

Fig. 3.5 Plot of the non-dimensional CMOD compliance function of 3-pt bend geometry as a function of normalized crack length α, showing the compliance function derived from Eq. (3.13) (solid circles), as compared to the solution according to ASTM E399 (solid line).

Fig. 4.1. Single-edge notched four-point bending SE(B) specimen with minor span to width ratio of 2. To measure the elastic compliance, a strain gauge was placed at the center of the back face, a double-cantilever clip-in displacement gauge was placed across the crack mouth, and a single-cantilever displacement gage was placed on one of the loading points at the major span. The details of the crack-mouth geometry are identical to that specified in ASTM E 399.

Fig. 4.2. Plot of the crack-mouth opening displacement compliance calibration, as a function of crack length, for the single-edge notched four-point bend specimen ($d/W = 2$) showing both the experimental data (open circles) and the numerical solution (filled circles), as compared to Tarafder *et al*.'s finite-element solution (solid line) [7]. The numerical compliance calibration for $d/W = 4$ is included for comparison [5, 6, 11].

Fig. 4.3. Plot of the back-face strain compliance calibration, as a function of crack length, for the single-edge notched four-point bend specimen ($d/W = 2$) showing both the experimental data (open circles) and the numerical solution (filled circles), along with the polynomial fit function (solid line). The numerical and experimental compliance calibration for $d/W = 4$ is included for comparison [9].

Fig. 4.4. Plot of the 4PB ($d/W = 2$) load-point displacement compliance calibration, as a function of crack length, for the single-edge notched four-point bend specimen ($d/W = 2$) showing both the numerical solution (filled circles) and the polynomial-fit function (solid line).

Fig. 4.5. The geometric function for calculating the linear-elastic stress-intensity factor for the single-edge notched four-point bend specimen with the minor span to width ratio of $d/W = 2$. The solid line represents the solution derived from CMOD compliance by Eq. (4.9), and the filled circles represent the solution derived from the load-point displacement solutions computed in this study.

LIST OF TABLES

Table 2.1 Comparison of Dugdale and Barenblatt's cohesive zone models

Table 3.1 Comparison of geometric functions, weight functions and compliance functions.

Table 4.1. Coefficients for crack-mouth opening displacement compliance calibration function: $\frac{EBW\delta}{M} = 24\sum_{i=0}^{5}\beta_i\alpha^{i+1}$, and the inverse CMOD compliance calibration function for crack length measurement: $\frac{a}{W} = \sum_{i=0}^{5}\beta_i' U^i$, where $U = \frac{1}{\sqrt{EBW\delta/M}+1}$, for $0.3 \le a/W \le 0.8$.

Table 4.2. Coefficients for back-face elastic strain compliance calibration function: $-\frac{EBW^2\varepsilon}{M} = 6\sum_{i=0}^{6}\beta_i\alpha^i$, and the inverse back-face strain compliance calibration function for crack length measurement: $\frac{a}{W} = \sum_{i=0}^{6}\beta_i' U^i$, where $U = \frac{1}{\sqrt{-EBW^2\varepsilon/M}+1}$, for $0.3 \le a/W \le 0.8$.

Table 4.3. Coefficients for load-line displacement compliance calibration function: $\frac{EB\Delta}{P} = 6\sum_{i=0}^{6}\beta_i\alpha^i$, and the inverse CMOD compliance calibration function for crack length measurement: $\frac{a}{W} = \sum_{i=0}^{6}\beta_i' U^i$, where $U = \frac{1}{\sqrt{EB\Delta/P}+1}$, for $0.3 \le a/W \le 0.8$.

ACKNOWLEDGEMENTS

I would like to thank my advisor, Professor Robert O. Ritchie, for giving me the freedom to explore my interest. This work would not be possible without Rob's encouragement and guidance. I am also grateful to Professor Papadopoulos, Professor Govindjee, and Professor Steigmann for their excellent instructions in solid mechanics. More specifically, Professor Papadopoulos' exceptional teaching aroused my interest in applying continuum mechanics in fracture mechanics; as a result, it leads to the current work. Many thanks go to Paul Novak who did the FEM simulation on the numerical compliance solutions for the four-point bend geometry, and Henry Wu who did the experiments with me on the compliance functions for this geometry. Thanks for helpful discussion are primarily due to my former group members, Dr. Brad Boyce and Dr. Jay Kruzic, and to my friend Dah-Wei Chiou. Last but never the less, I want to thank my parents and my husband for their patience and love.

CHAPTER 1

SYNOPSIS

Fracture mechanics introduces the concept of fracture toughness into engineering design. Fracture toughness relates the strength of a load bearing structure to the dominant crack size contained in that structure. Consequently, one of the essential ingredients in fracture mechanics based analysis is to determine the crack size and the stress intensity factor at the crack tip [1]. Geometric functions, weight functions and compliance functions in linear elastic fracture mechanics (LEFM) have been intensively studied for use in determining these essential values. The geometric function is employed to determine the stress intensity factor in a relatively simple stress state, e.g. a far field uniform stress or single point load; whereas the weight function gives a way to determine the stress intensity factor even in complicated stress states. The compliance function is used to determine the crack length.

Although the above functions have been well developed for different testing geometries and are widely available in handbooks for researchers and engineers, there have been no investigations into the relations between them except the known correlation between the geometric function and the load-point compliance function [2, 3]. Therefore, the purpose of this work is to investigate the intrinsic relations between geometric functions, weight functions and compliance functions in the framework of LEFM and to simplify the numerical process in obtaining such functions. A brief introduction to fracture mechanics is presented in Chapter 2, discussing its definition and historical perspectives. The relations between the three functions will be studied in Chapter 3. An

example on bending geometry will be given in Chapter 4 to illustrate the application of the relations between these functions. Finally, conclusions will be drawn with some suggestions for future work.

REFERENCES

1. X.-R. Wu and A.J. Carlsson, *Weight Functions and Stress Intensity Factor Solutions*. 1st ed: Pergamon Press. 1991, 513 p.
2. H. Tada, P.C. Paris, and G.R. Irwin, eds. *The stress analysis of cracks handbook*. 3rd ed. ASME Press.2000, 677 p.
3. J.W. Hutchinson, *A course on nonlinear fracture mechanics*: Technical University of Denmark. 1979, 101 p.

CHAPTER 2

BACKGROUND ON FRACTURE MECHANICS

2.1 SCOPE AND DEFINITION

As an interdisciplinary field of materials science and applied mechanics, fracture mechanics employs continuum mechanics to quantify "the conditions under which a load-bearing structure fails due to an enlargement of a dominant crack contained in that body" [1]. The definition may be understood in the following terms.

First, fracture mechanics is different from other structural analysis methods because it assumes that defects already exist in any material and they invariably lead to failure. Furthermore, the failure originates from only one major crack. Even though other defects exist, they are not supposed to initiate nor propagate in the presence of applied loads. Thus fracture mechanics is only applicable to analyze results from tests where a crack has to preexist. For the same reason, all the standard fracture mechanics-based specimens have a notch as the major dominant crack/defect.

Second, size effects are important in fracture since it is a phenomena occurring at multiple scales, from the atomic bond rupture at the angstrom scale, to dislocation motion involving hundreds of atoms, to cracking along grain boundaries at the micron scale, and to failure due to improper structure design at a large scale. Usually only failure at one scale dominates the whole fracture process and the critical scale changes with the size of the structure in the application. It is the materials scientist's goal to find out this scale and identify failure mechanisms for different material system under different testing environments. It is the mechanics theoretician's work to define the boundaries within

which scale the continuum mechanics apply and how all the properties and failure conditions determined from small-scale laboratory tests should be used in the scales of application.

Third, quantification is one of the main goals of modern science. Without it, application would not be possible. Failure conditions at different scales are quantified through different analytical models. Under macroscopic conditions, the failure condition is quantified with continuum mechanics in terms of energy or load, etc. Under microscopic conditions, a micro-mechanical model is established based on the failure mechanism at the critical scale. For example, the failure mechanism in the ductile fracture of mild steels is identified as transgranular fracture, where the movement of dislocations is assumed to cause the failure. Correspondingly, the micro-mechanics criterion for this mechanism is that the crack will initiate once the strain at the crack tip exceeds a maximum value.

As depicted in Fig. 2.1, fracture mechanics is constituted of three elements: microstructure (materials), testing conditions (application requirements), and analytical models (both continuum mechanics and micro-mechanics). Fracture properties are calculated from the measured quantities in the tests with these models. Since a property is a material's response to some external stimuli, different combinations of microstructure and testing conditions require different macroscopic and micro-mechanical models to obtain the fracture properties.

Contributions from two fields are required to understand fracture. In the materials science field, the failure mechanism needs to be identified at the critical size scale to provide an understanding on the microstructure-mechanism-property relationship. In the

mechanics field, macroscopic and micromechanical analytical models should be established based on observations and the failure mechanism to provide proper quantification. Since the mechanism varies with different materials and different testing conditions, only the mechanics part will be reviewed.

In the mechanics part, two basic tools are employed to quantify the failure conditions in fracture mechanics: thermodynamics and constitutive laws in continuum mechanics. By way of the first law in thermodynamics, crack length is related to energy through mechanical energy balance. By way of different constitutive laws, failure connects energy terms with stress. Thus energy becomes the bridge connecting the stress and the crack length. This stress-energy-crack relation is also the essence of fracture mechanics. Below is a brief account of the theoretical part of fracture mechanics from two perspectives: the energy balance of a cracked system and the irreversibility of the crack propagation determined by thermodynamics, and the stress/displacement solutions at crack tip due to different constitutive laws.

2.2 THERMODYNAMICS IN FRACTURE MECHANICS

2.2.1 Some Terms in Thermodynamics

Thermodynamics studies the mass and energy exchange between a system and its environment, as well as the energy conversion inside a system. It only applies to systems *in equilibrium* that can be fully described by a few macroscopic thermodynamics properties. For example, ideal gas can be studied by thermodynamics; whereas a computer cannot. Before thermodynamics is applied to cracking problems, a few terms in thermodynamics need to be clarified for later discussion.

2.2.1.1 State Functions and Transitional Quantities

Thermodynamics relates the seemingly irrelevant quantities such as temperature, pressure, and chemical potential, etc. through energy, or state functions. State means a set of thermodynamic properties that describe a system in equilibrium. State functions are different energy expressions in terms of these properties. Typical state functions for solids are internal energy and Helmholtz free energy. As mentioned earlier, thermodynamics studies the mass and energy exchange between different equilibrium states. The energy exchange between states is accomplished through work and heat. Work and heat are means of energy transfer between states but they are not state functions. They usually cannot be expressed as a function of thermodynamic properties, only except during quasi-static transitions.

2.2.1.2 Quasi-Static vs. Reversible Transitions

Quasi-static transition is composed of continuous equilibrium states. Only in this condition can work and heat be expressed by thermodynamic quantities according to the first law. Reversible transition requires that both system and environment can return to their original states. Reversible transition is always a quasi-static transition but the reverse is not true.

2.2.2 Energy Release Rate by the First Law

2.2.2.1 Energy Release Rate and Fracture Criteria

Consider a *quasi-static* crack propagation process in a *time-independent elastic* solid body from crack size a_1 (Fig. 2.2a) to a_2 (Fig. 2.2d). From the first law, the internal energy change of the cracked body comes from the mechanical work and heat exchange with the environment;

$$dU = \delta W + \delta Q\,, \tag{2.1}$$

where U is the internal energy, W is the work done on the system, Q is the heat exchange between the cracked body and the environment, d means the differential of state functions, and δ means the change of transitional quantities since work and heat are usually not state functions. Then the question is how to determine the three terms in Eq. (2.1) by thermodynamic properties and experimentally measured quantities.

In the left side of Eq. (2.1), the internal energy of the cracked body can be fully described by temperature, entropy, elastic strain energy, crack area, and the surface energy at crack surfaces. Thus the change of the internal energy due to crack propagation in presence of load can be expressed as:

$$dU = T\,dS + dU_{strain}^{elastic} + \gamma\, d(2A)\,, \tag{2.2}$$

where T is temperature, S is entropy, $U_{strain}^{elastic}$ is the elastic strain energy caused by external loading, γ is the surface energy at crack surfaces, and A is the crack area on one side.

In the right side of Eq. (2.1), the work done on the system in a *quasi-static* process can be calculated from the load and displacement curve (as shown in Fig 2.2 e).

$$\delta W = dW = P d\Delta\,, \tag{2.3}$$

where P is the load, Δ is the total displacement at loading points. The heat exchange in a *quasi-static* process is

$$dQ = T dS\,. \tag{2.4}$$

Substituting Eqs. (2.2-4) into (2.1) and reforming it lead to

$$dW - dU_{strain}^{elastic} = 2\gamma\, dA\,. \tag{2.5}$$

Obviously, the condition *quasi-static* process eliminates the effect of heat to the cracking process, thereby reducing the first law to a simple mechanical work balance containing the information of crack size. Further derivative of the left side of Eq. (2.5) with respect to the crack area leads to the definition of energy release rate (or crack driving force) $\mathcal{G}$ as:

$$\mathcal{G} = \frac{d\mathcal{W} - dU^{elastic}_{strain}}{dA}. \tag{2.6}$$

The right side of Eq. (2.5) is considered as fracture resistance $\mathcal{R}$. In time-independent elasticity, this resistance is twice the surface energy:

$$\mathcal{R} = 2\gamma. \tag{2.7}$$

Fracture resistance is not necessarily the surface energy. It varies with the constitutive behavior of the material.

As a result the fracture criteria are based on energy release rate $\mathcal{G}$ and fracture resistance $\mathcal{R}$ as

$$\mathcal{G} \geq \mathcal{R} \text{ (initiation)}, \tag{2.8}$$

and

$$\frac{d\mathcal{G}}{dA} > \frac{d\mathcal{R}}{dA} \text{ (propagation)}. \tag{2.9}$$

Eqs. (2.6, 8-9) hold not only elasticity, but also plasticity. In elasticity, fracture resistance is a property; in plasticity, fracture resistance R is Fracture resistance is not necessarily the surface energy or a constant.

2.2.2.2 Meaning of the Energy Release Rate

Energy release rate can be understood in the following aspects.

As shown in the loading/unloading cycle of a cracked body (Fig. 2.2), the external work equals to the inside elastic strain energy when the crack is about to propagate (Fig. 2.2b). After propagation, the external work is used to create new crack surfaces and cause elastic strain inside the body at new crack length (Fig. 2.2c). Upon unloading, elastic strain is released. The energy difference between the states in Fig. 2.2a and 2.2d is just the energy for creating the new crack area, also the net work done on the system (or the area enclosed by the loading/unloading displacement curve) according to Eq. (2.5). So the net work done on the system after a loading/unloading cycle overcomes the resistance for crack propagation.

A second view of the energy release rate is from the virtual work. As mentioned earlier, the external work, or the actual work, is the area under a loading path in a quasi-static process. It is expressed as

$$\mathcal{W} = \int_{\Delta} P d\Delta', \tag{2.10}$$

Virtual work $\mathcal{V}$ is defined as the direct product of load and corresponding displacement regardless of the change of the load;

$$\mathcal{V} = P\Delta. \tag{2.11}$$

Notwithstanding the different concept, the incremental forms of the two work expressions are the same under constant load;

$$d\mathcal{W}\big|_P = d\mathcal{V} = Pd\Delta, \tag{2.12}$$

where the subscript P means constant load control. Thus the energy release rate or crack driving force under constant load control can also be expressed as

$$\mathcal{G} = \frac{d(\mathcal{V} - \mathcal{U}_{strain}^{elastic})}{dA} = \frac{dU_{strain}^{*}}{dA} = -\frac{d\Pi}{dA}, \tag{2.13}$$

where U_{strain}^{*} is the complimentary strain energy, defined as

$$U_{strain}^{*} = V - U_{strain}^{elastic}, \tag{2.14}$$

and Π is the potential energy, defined as

$$\Pi = U_{strain}^{elastic} - V. \tag{2.15}$$

From Fig. 2.2e, potential energy and complimentary strain energy denotes the same area except the signs are opposite. So the energy release rate is also the change of the complimentary energy (or potential energy) with respect to the extension of crack. A third view of the energy release rate is by J-integral, which will be discussed in section 2.2.3.3.

With the expression of energy release rate determined, the work is calculated from the loading curve, and the strain energy is calculated based on different constitutive laws of the material. Particularly in linear elasticity, Claypeyron theorem [2] indicates that the virtual work is twice the elastic strain energy, so the energy release rate is further simplified to

$$\mathcal{G} = \left.\frac{dU_{strain}^{elastic}}{dA}\right|_{\Delta} = \left.\frac{1}{2}\frac{dV}{dA}\right|_{P}, \tag{2.16}$$

where the subscript Δ means constant displacement control (or fixed boundaries). So the energy release rate in linear elastic fracture is either the elastic strain energy release rate

under constant displacement control, or half the virtual work release rate under constant loading control.

2.2.3 Historical Review on Energy Release Rate

A brief review on the concept energy release rate is presented in this section with a focus on the postulates, contributions and limitations.

2.2.3.1 Griffith's Work in Elasticity

Strength or maximum strain was recognized as the single parameter controlling fracture events in nineteenth century. It was assumed that a structure failed once the stress or strain exceeded a critical value. This concept was not challenged until Griffith employed the energy conservation and Inglis' stress analysis to study the failure strength of a cracked elastic plate in the 1920s [3-5].

A. Postulates and Formulation

Griffith considered a quasi-static propagation process in a cracked linear-elastic plate subject to far-field uniform tension. Using the energy balance, he derived the expression of energy release rate as shown in Eq. (2.6). He thought the fracture resistance for isotropic elastic material is just the surface energy and this surface energy should be a constant. With constant resistance, the initiation and propagation criteria are simplified to one equation, i.e.

$$\mathcal{G} > \mathcal{R} . \tag{2.17}$$

His criterion implicates that the crack simply propagated upon initiation, which is true in most brittle materials.

Griffith then employed Inglis' 2-D stress solution [3] to obtain an expression for the strain energy and established a relation between failure strength σ_F and the crack size through Eq. (2.16);

$$\sigma_F = \sqrt{\frac{4E\gamma}{\pi a}} = \sqrt{\frac{2E\mathcal{R}}{\pi a}}, \tag{2.18}$$

where E is Young's modulus either in plane strain ($E/(1-\nu^2)$) or plain stress (E) condition, ν is Poisson's ratio, and a is the crack size. Since Inglis' solution is for 2-D or 3-D cases where thickness is not a variable, the energy release rate is expressed in terms of crack size instead of crack area.

Griffith further extended his expression for failure strength to atomic scale. He replaced the crack length a with the atomic bond length ρ in Eq. (2.18) and obtained the so-called theoretical ultimate strength σ_{th}:

$$\sigma_{th} = \sqrt{\frac{4E\gamma}{\pi\rho}}. \tag{2.19}$$

Griffith searched literature on the surface energy for different materials and found the theoretical ultimate strength was about tenth of Young's modulus based on Eq. (2.19); $\sigma_{th} \sim E/10$. Therefore, the far-field failure strength for any cracked elastic material could be quickly determined from the size of the crack contained in that body:

$$\sigma_F = \sigma_{th}\sqrt{\frac{\rho}{a}} \sim \frac{E}{10}\sqrt{\frac{\rho}{a}}. \tag{2.20}$$

B. Contributions and Limitations

With the energy balance theorem and stress analysis, Griffith laid a solid foundation for fracture mechanics. He not only quantified the failure strength with respect to the

crack size, but also formulated the crack driving force from mechanical energy conservation. In addition, he recognized the surface energy as the fracture resistance in isotropic elastic material, and also formulated a criterion for crack initiation and propagation. His conclusion of the dependence of failure strength on crack size was verified by experiments on brittle materials. This success leads researchers to consider flaw size, instead of detailed microstructure parameters, as a dominant factor in determining the strength of brittle solids.

However, no attempt is perfect. Some limitations exist in Griffith's work.

First, Griffith stressed that his results were valid only for reversible crack propagation process. It is misleading. Quasi-static process can fully guarantee the validity of the mechanical energy balance, as discussed in section 2.2.2. This reversibility problem has been haunting researchers ever since Griffith's work and different theories has been yielded to try to reconcile the "admissible reversibility" with some contradicting experimental results. Thermodynamics itself does not specify whether the crack could reverse or not. Further research work needs to be done to understand the mechanism for this admissible reversibility.

Second, Griffith recognized surface energy as the source of fracture resistance. Experiments on most metallic materials show much higher failure strength based on Eq. (2.18). It means that other energy dissipation processes occur during crack propagation rather than creating new surfaces.

Third, the expression for theoretical ultimate strength in Eq. (2.19) is controversial since continuum mechanics does not hold at atomic scale. Even if Eq. (2.19) was right, it has different meaning from Eq. (2.18). In Eq. (2.18), the crack with length a is the

largest flaw in the structure and there is only one such crack. This condition guarantees that cracking only occurs around the largest crack. In contrast, all the atoms have the same atomic distance (ρ). Therefore, Eq. (2.19) implies that all the atomic bonds rupture at the same time; a solid piece breaks into atoms instantly. This is an explosive manner and it rarely happens in practice.

2.2.3.2 Irwin's Modification for Plasticity

Griffith's work yields the correct functional relationship between failure stress and the crack/flaw size and it was verified by many results on brittle-behaving materials. However, results on small ductile-behaving test pieces showed extensive plastic deformation and the failure strength value was much higher than the one given by Eq. (2.19). To solve this problem, Irwin introduced included the plastic deformation in the sources of fracture resistance.

A. Formulation

In time-independent deformation, strain energy stored in a loaded structure is composed of two parts: elastic strain energy that can be released during unloading, and plastic strain energy ($U_{strain}^{plastic}$) that remains inside the structure even after unloading. Correspondingly the internal energy of a cracked structure is expressed as

$$dU = T\,dS + dU_{strain}^{elastic} + dU_{strain}^{plastic} + \gamma\, d(2A)\,. \tag{2.21}$$

The energy release rate is defined in the same manner as in Eqs. (2.6,13). On the contrary, the expression for fracture resistance with plasticity becomes:

$$\mathcal{R} = 2\gamma + \frac{dU_{strain}^{plastic}}{dA} = 2\gamma + \gamma^{plastic}\,, \tag{2.22}$$

where $\gamma^{plastic}$ is defined as the plastic strain energy per unit crack area.

Irwin recognized the plastic deformation as part of the fracture resistance and simply replaced the term $\mathcal{R}$ in Eq. (2.19) with (2.22). The failure strength in the presence of plasticity becomes:

$$\sigma_F = \sqrt{\frac{2E\mathcal{R}}{\pi a}} = \sqrt{\frac{2E(2\gamma + \gamma^{plastic})}{\pi a}} \tag{2.23}$$

B. Contributions and Limitations

Irwin's tentative work on plasticity recognized the plastic deformation as the source of the fracture resistance; however, it is successful due to the following problems.

First, by simply adding the plastic deformation into the resistance, Irwin assumed that Inglis' solution still held in the plastically deformed body. However, the stress distribution inside the structure changes when plasticity occurs. So Eq. (2.23) does not give a correct quantification of the failure strength with crack size.

Second, Irwin did not give a recipe for measuring the plastic deformation, which made the experimental verification impossible.

Third, one important aspect of fracture mechanics is that all the properties and failure conditions determined from small-scale laboratory tests should be the same as used in the scales of application. Since the elastic deformation is released during unloading, extrapolation to different scales is not a problem in elasticity once the theory of elasticity still holds. In plasticity, however, size-dependent problem arises because the plastic deformation remains in the structure upon unloading and amount of permanent deformation varies with the size of the structure. This means the resistance quantified from a laboratory specimen is only meaningful to that size, but loses the extrapolation to other scales. Consequently, researchers have made distinction between small scale

yielding and large scale yielding. Fracture properties (or failure conditions) under small scale yielding can be applied to structures at different size scales because the plastic deformation zone is so small compared to the size of the loaded structure that the amount of plastic deformation is invariant for a structure of different size scales. On the contrary, fracture properties under large scale yielding lose the extrapolation to other size scales.

2.2.3.3 J-integral Method

A. Formulation

Independent of Eshelby's work, Rice proposed a path independent J-integral as the energy release. Rice considered a 2-D case (Fig. 2.3) where J-integral is defined as [6]

$$J = \int_{\Gamma_0} (w\,dx_2 - t_i \frac{\partial u_i}{\partial x_1} dl), \tag{2.24}$$

where w is the strain energy density, x_1, x_2 are Cartesian coordinates, i is the index for Cartesian coordinates, Γ_0 is the boundary of the test piece that starts from one end of the crack surface and ends at the opposite side, t is the traction acting on Γ_0, u is the displacement, and l is the length of the boundary Γ_0. Note that Γ_0 is not a closed path.

J-integral is in nature the strain energy release rate derived from the complimentary strain energy (Eq. (2.13)) by Green and Gauss's theorems;

$$\mathcal{G} = \frac{d(\int_{\Gamma_0} t_i u_i dl - \int_{\Omega} w d\Omega)}{da} = \int_{\Gamma_0} (w\,dx_2 - t_i \frac{\partial u_i}{\partial x_1} dl) = J\,. \tag{2.25}$$

Detailed proof of Eq. (2.25) is provided by Kanninen [1]. Rice further proved that J-integral of any closed loop in an elastic field is zero. The energy release rate can be evaluated from any path in an elastic field on the specimen by Eq. (2.24).

B. Discussion

J-integral was considered as a generalized energy release rate for any cases [7]; however it is not true. J-integral has the following restrictions. i) It is only applicable to small scale yielding elastic-plastic 2-D fields, or 3-D structures where thickness has to be constant. The derivation of Eq. (2.25) involves linear coordinate transformation. The deformation has to be small so that the coordinate transformation is still linear in scales. ii) J-integral is path independent only on condition that the integrand in Eq. (2.24) has no singularity and the integral is bounded along any path in an elastic field. For example, J-integral is zero along Γ_0-crack surfaces-Γ_1 or Γ_1-crack surfaces-Γ_2 (Fig. 2.3), where Γ_1 is an arbitrary path, and Γ_2 is the elastic-plastic interface. Crack tip is considered a singularity although the integral is bounded at the tip. Therefore the J-integral is not zero along a closed path containing crack tip (Γ_2-crack surfaces), but the energy release rate. iii) The path can only lie in elastic field and cannot cross the plastic-elastic boundary.

Besides the energy release rate, J-integral also means the energy flow across the selected path into the specimen, or the net work done during a loading/unloading cycle in a closed path. Consider the closed path Γ_0-crack surfaces. After crack propagation, the energy left in the path is the energy for plastic deformation in the plastic zone (enclosed by Γ_2-crack surfaces) and for creating new crack surfaces, which is just the net work done in Fig. 2.2e.

By the first law of thermodynamics, energy release rate is formulated in a quasi-static crack propagation process in a time-independent deformable structure with small scale yielding. Eqs. (6,13) are expressions for a general 3-D case, whereas J-integral is only

for 2-D structure. In addition, crack initiation and propagation criteria are also proposed (Eq.s (2.8-9)).

2.3 CONSTITUTIVE LAWS

Constitutive laws are the other important factor in the theory of fracture mechanics because they are used not only to determine the strain energy for the energy release rate, but also to yield the stress/displacement solutions in the structure. The stress/displacement fields at crack tip are of particular interest since they help to understand the microstructure behavior. Consequently, the stress solutions at crack tip are summarized for elastic, and elastic-plastic with small scale yielding fields. Emphasis is placed on the postulates, but not the derivation or solutions.

2.3.1 Linear Elasticity

In linear elasticity, the displacement and stress solutions of an isotropic body at crack tip can be determined by complex variable method[5, 8] in a 2-D plane. The solutions take the following form near the crack tip:

$$u_i = K_\alpha \sqrt{\frac{r}{2\pi}} \Psi_i(\theta) + \mathrm{O}(\sqrt{r}), \tag{2.26}$$

and

$$\sigma_{ij} = \frac{K_\alpha}{\sqrt{2\pi r}} \Theta_{ij}(\theta) + \mathrm{O}(\sqrt{r}), \tag{2.27}$$

where σ is the stress, K is an undetermined constant controlling the magnitude of the stress and the displacement at the crack tip, α represents the loading mode of tension, shear, and tear, respectively, r and θ are the polar coordinates with crack tip as the origin, i and j are indices for either Cartesian or polar coordinate system, Ψ(θ) and Θ*(θ)* are the

angular dependence respectively for displacement and stress distribution, and $O(\sqrt{r})$ represents the higher-order terms of $\sqrt{r}$.

Irwin [9] ignored the higher-order terms in Eqs. (2.26-27) and integrated the work needed to form a new crack. By this way, the undetermined constants are found to be related with the energy release rate in the following way:

$$\frac{K_I^2 + K_{II}^2}{E} + \frac{K_{III}^2}{2\mu} = \mathcal{G}, \tag{2.28}$$

where μ is the shear modulus. K is therefore defined as stress intensity factor, linking important quantities at different scales. At macroscopic scale, K^2/E is the energy release rate, the driving force applied to the elastic body; at microscopic scale, K determines the amplitude of the stress at the crack tip. Thus the loading conditions for each crack length could be calculated from stress intensity factor, instead of crack driving force.

According to Eq. (2.27), the stress becomes infinite large at the crack tip. This is impossible in real materials since they would yield first at certain stress. Then small scale yielding at the crack tip is considered to modify this unbounded solution from linear elasticity.

2.3.2 Linear Elasticity-Perfect Plasticity

To solve the singularity of the stress solution at the crack tip, linear elasticity-perfect plasticity is considered at the crack tip. The constitutive behavior is shown in Fig. 2.4. Only case in Mode I is considered.

2.3.2.1 Irwin's Solution

Irwin only considered the normal stress at the crack tip and formulated a force balance in uniform tension (Fig. 2.5). In the presence of plasticity, the stress at the crack

tip is the yield strength σ_Y in the plastic zone with a size of r_P, and takes the form of elastic solution (Eq. (2.27)) in the elastic zone. The elastic solution of the normal stress σ_{yy} near the crack tip along the crack is (θ = 0):

$$\sigma_{yy} = \frac{K_I}{\sqrt{2\pi r}}. \tag{2.29}$$

In plane stress condition, the characteristic length r_Y at yielding is solved from Eq. (2.29),

$$r_Y = \frac{1}{2\pi}(\frac{K_I}{\sigma_Y})^2. \tag{2.30}$$

Force balance in y-direction requires that the area under the broken curve ($\frac{K}{\sqrt{2\pi r}}$) is the same as under the solid curve. Therefore, the two gridded regions should have the same area;

$$\sigma_Y r_P = \int_0^{r_Y} \sigma_{yy} dr. \tag{2.31}$$

Combining Eqs. (2.29-31) lead to:

$$r_P = 2r_Y = \frac{1}{\pi}(\frac{K_I}{\sigma_Y})^2. \tag{2.32}$$

The stress solution in the elastic region can be viewed as if the origin shifted with a length of r_y. Therefore, Irwin's stress solution (in plane stress condition) for single normal stress in presence of the perfect plasticity is:

$$\sigma_{yy}(\theta = 0) = \begin{cases} \sigma_Y, & r \le r_P \\ \dfrac{K_{eff}}{\sqrt{2\pi(r - r_Y)}}, & r > r_P \end{cases} \tag{2.33}$$

Irwin ignored the triaxial stress distribution at the crack tip and only considered a single force balance in tension direction. He also assumed that the elastic stress outside

the elastic zone still took the same form as the solution in linear elasticity. His analysis implies that the crack tends to be blunt in the presence of plasticity, so that the crack seems to be longer. These implications were verified by Wells' experimental observation [10].

2.3.2.2 Von Mises Yield Criterion

This method considers the triaxial stress state at the crack tip. For multiple stress state, yielding occurs once the effective strength σ_e exceeds the yield strength σ_Y determined under uniform tension according to von Mises criterion. The effective strength is defined as:

$$\sigma_e = \frac{1}{\sqrt{2}}[(\sigma_1 - \sigma_2)^2 + (\sigma_2 - \sigma_3)^2 + (\sigma_3 - \sigma_1)^2]^{1/2}, \qquad (2.34)$$

where σ_1, σ_2, and σ_3 are the three principal normal stresses determined from the triaxial stress at the crack tip by Mohr's circle. In perfect plasticity, the plastic zone under mode I determined from Eq. (2.34) is shown in Fig. 2.6.

Linear elasticity-strain hardening plasticity is also considered for the stress solutions at the crack tip. The details can be found in any books on advanced fracture mechanics [1, 7].

2.3.3 Cohesive Zone Models

Cohesive zone models assume that a zone with cohesive stress exists ahead of the crack tip. Dugdale [11] prescribed the shape of the cohesive zone and the proposed a stress distribution inside the cohesive zone. With the above postulates, he derived the length of the cohesive zone in terms of applied stress, yield strength, and the crack size. Barenblatt [12] did not prescribe the shape of the cohesive zone or assume any stress

distribution inside the zone. He deemed the work to open the cohesive zone as the source of the crack resistance. With energy balance and boundary conditions he derived the stress and displacement solutions inside the cohesive zone. The comparison of the two models is listed in Table 2.1. A brief account of the two models is presented below with an emphasis on postulates and assumptions. Note that all the solutions are under Mode I.

2.3.3.1 Dugdale's Model: Linear Elasticity-Perfect Plasticity

Dugdale's cohesive zone model [11] has the following postulates. i) The normal stress σ_{yy} ahead of the crack is the dominant stress responsible for crack propagation under mode I. ii) a plastic zone of length *d* with constant stress σ_Y exists ahead of the crack tip. The shape of the zone is determined by the following conditions. iii) The experiment was performed on thin steel plate (Fig. 2.7a) so the plane stress condition holds ($\sigma_{zz} = 0$). iv) He considered the steel as a linear elastic-perfectly plastic material. By Tresca yield criterion and Mohr's circle method, the shear stress lies in the x2-x3 plane at 45 degrees to x2 coordinates (Fig. 2.7b). Therefore, the height of the zone is the same as the thickness of the plate. v) The length of the cohesive zone d is determined from Muskhelishvili's solution [11] as a function of far-field applied stress σ_A, yield strength σ_Y, and crack size *a*.

Dugdale performed a series of tests on steel sheets with varying applied stress and crack size. The experimental results of the plastic zone length d agreed well with the prediction values solved by Muskhelishvili's method.

2.3.3.2 Barenblatt's Work

Barenblatt [12] also assumed a cohesive zone existed ahead of the crack tip. Different from Dugdale, he did not specify the shape of the plastic zone or the stress

distribution inside the zone. His work is based on three hypotheses: i) the length of the cohesive zone (d) is small compared to the size of the crack; and ii) the stress distribution $p(r)$ (not specified) inside the cohesive zone is invariant regardless of the external loading conditions (magnitude of the load, loading positions and so on). iii) The cohesive stress must satisfy the following relation:

$$\int_0^d p(r)d(\sqrt{r}) = K_I \tag{2.35}$$

By Eq. (2.35), Barenblatt implied the linear elastic nature of the cohesive stress by default although the stress value exceeds the yield strength. He also recognized that the fracture resistance should come from the cohesive zone. With Eq. (2.35) and other boundary conditions, Barenblatt derived solutions for stress and displacement fields in the cohesive zone.

2.4 SUMMARY

My view of fracture mechanics was presented in this chapter. A definition of fracture mechanics and its scope were discussed first, followed by the theory of fracture mechanics reviewed from two aspects: energy and constitutive laws. In the view of energy balance, the concept of energy release rate was developed from the first law of thermodynamics. In the view of constitutive laws, stress solutions at crack tip for different material behaviors were discussed. These models are all for quasi-static crack propagation in time-independent deformable solids with small scale yielding. With the theoretical background laid for fracture mechanics in this chapter, linear elastic fracture mechanics will be investigated in detail in the next chapter with a focus on some special functions for quantifying the energy release rate (or stress intensity factors).

REFERENCES

1. Kanninen, M. and C. Popelar, *Advanced fracture mechanics*. Oxford engineering science series. 1985: Oxford University Press.
2. Sokolnikoff, I.S., *Mathematical theory of elasticity*. 2nd ed. 1956: McGraw-Hill Book Company. 476 p.
3. Griffith, A.A., *The phenomena of rupture and flow in solids.* Philosophical Transactions of the Royal Society, 1920. **A221**: p. 163.
4. Lawn, B., *Fracture of brittle solids*. 1993: Cambridge University Press. 378 p.
5. Anderson, T.L., *Fracture mechanics : fundamentals and applications*. 2nd ed. 1995: CRC Press. 688 p.
6. Rice, J.R., *A path independent integral and the approximate analysis of strain concentration by notches and cracks.* Journal of Applied Mechanics, 1968. **35**(2): p. 379-86.
7. Hutchinson, J.W., *A course on nonlinear fracture mechanics*. 1979: Technical University of Denmark. 101 p.
8. Knott, J.F., *Fundamentals of fracture mechanics*. 1973: Butterworths. 273 p.
9. Irwin, G.R., *Analysis of stresses and strains near the end of a crack traversing a plate.* Transactions, Am. Soc. Mechanical Engrs., Journal of Applied Mechanics, 1957.
10. Wells, A.A. *Unstable Crack Propagation in Metals: Cleavage and Fast Fracture*. in *Proceedings of the crack propagation symposium*. 1961. Cranfield, UK.
11. Dugdale, D.S., *Yielding of steel sheets containing slits.* Journal of Mechanics and Physics of Solids, 1960. **8**: p. 100-104.
12. Barenblatt, G.I., *The mathematical theory of equilibrium cracks in brittle fracture.* Advances in Applied Mechanics, 1962. **7**: p. 55-129.

TABLES AND FIGURES

Table 2.1 Comparison of Dugdale and Barenblatt's cohesive zone models

	Dugdale	Barenblatt
2-D problem	Plane stress condition	Either plane stress or plane strain condition
Cohesive zone shape	Height is the same as thickness. Length d is a function of a, σ_A, σ_Y	Not specified, but length $d << a$
Constitutive law	Linear elasticity-perfect plasticity	Linear elasticity
Method	Muskhelishvili's method	Not specified, but solved by Eq. (2.35) and BCs*.
Cohesive stress	Constant, σ_Y	Not constant

* BCs means boundary conditions.

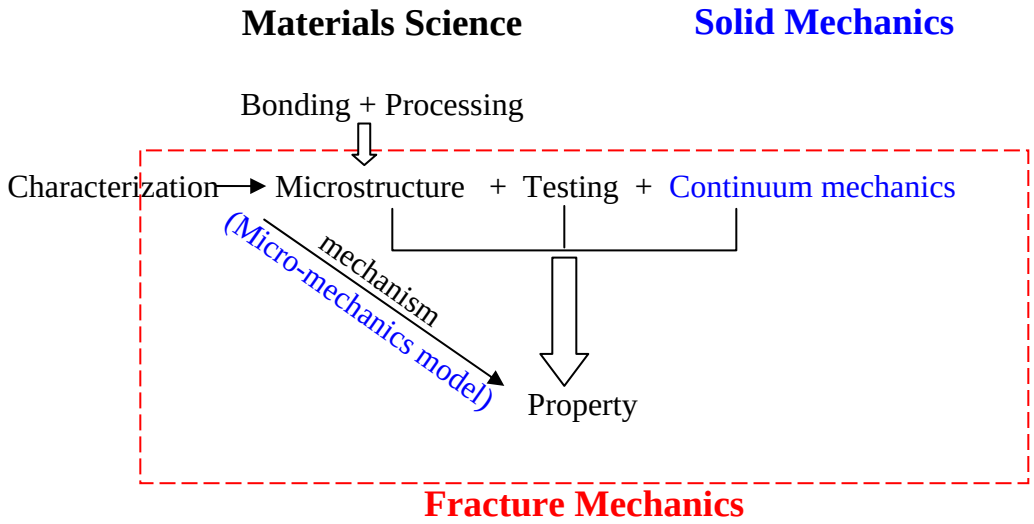

Fig. 2.1 Scheme of fracture mechanics as an interdisciplinary field of materials science and solid mechanics.

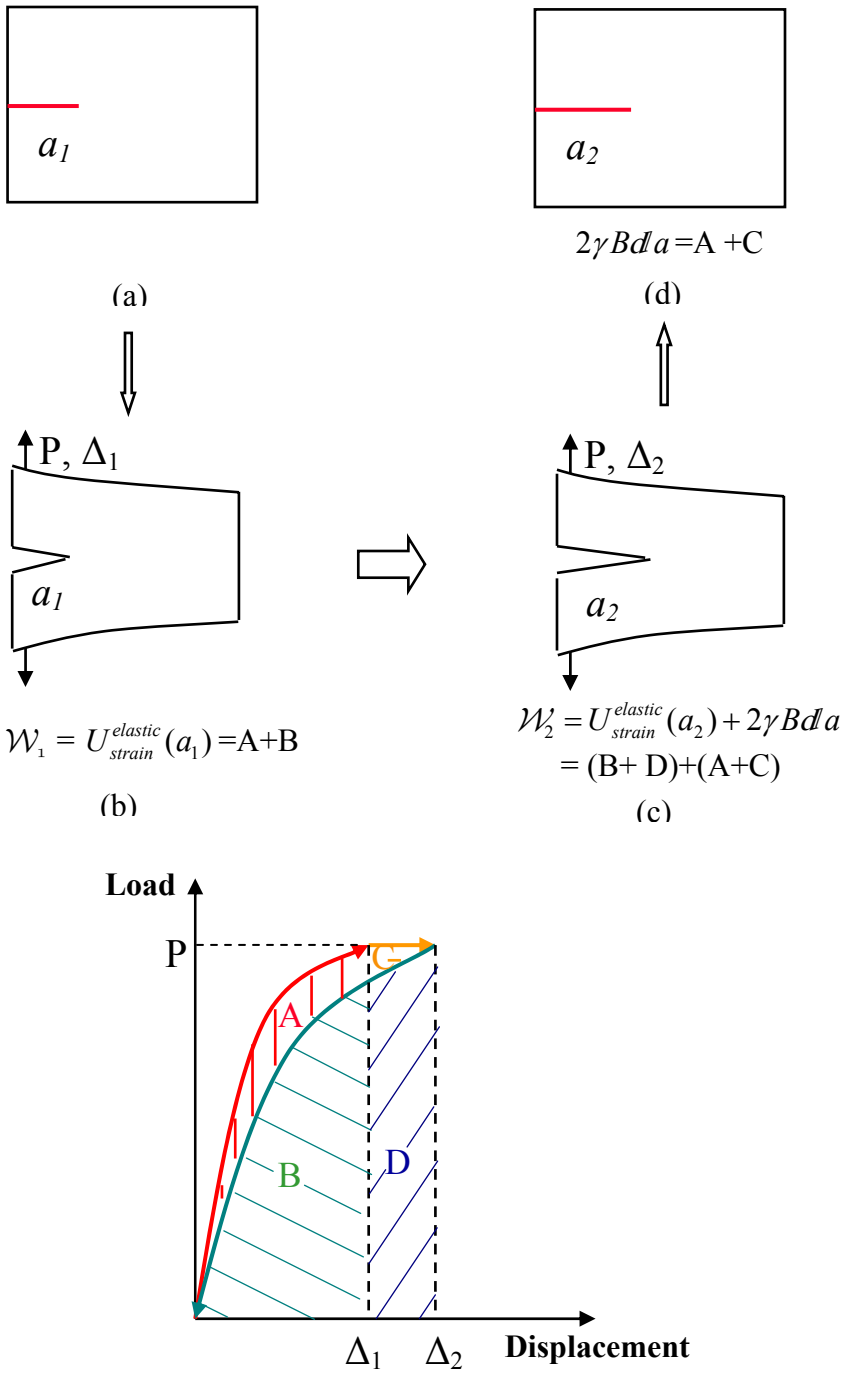

(e) Load-displacement curve of a loading-unloading cycle in a cracked elastic body.

Fig. 2.2 A quasi-static crack propagation in a cracked elastic body from crack size a_1 (a) to a_2 (d) after a loading-unloading cycle (e). When the crack is about to propagate (b), the external work done on the system is balanced by the elastic strain energy (area A and B). After propagation, the external work is balanced by the elastic strain energy (area B and D) at the new crack length and the surface energy of the new crack (area A and C).

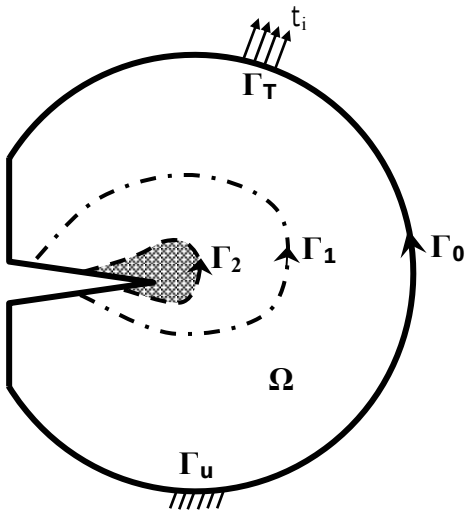

Fig. 2.3 A cracked 2-D elastic solid structure Ω, where Γ_0 is the boundary enclosing Ω except the crack surfaces, Γ_1 is an arbitrary path inside Ω, and Γ_2 is the elastic-plastic interface. The region enclosed by Γ_2 and the crack is the plastic deformation zone.

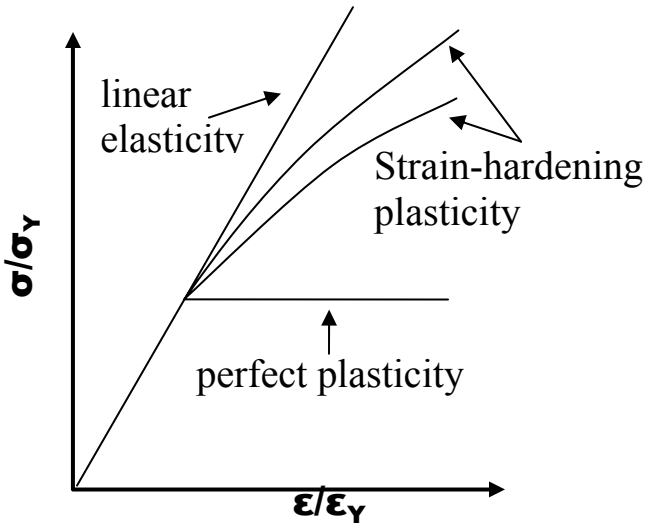

Fig. 2.4 Different constitutive behaviors of materials, where σ_Y is the yield strength determined from uniform tension test and ε_Y is the strain resulting from the yield strength.

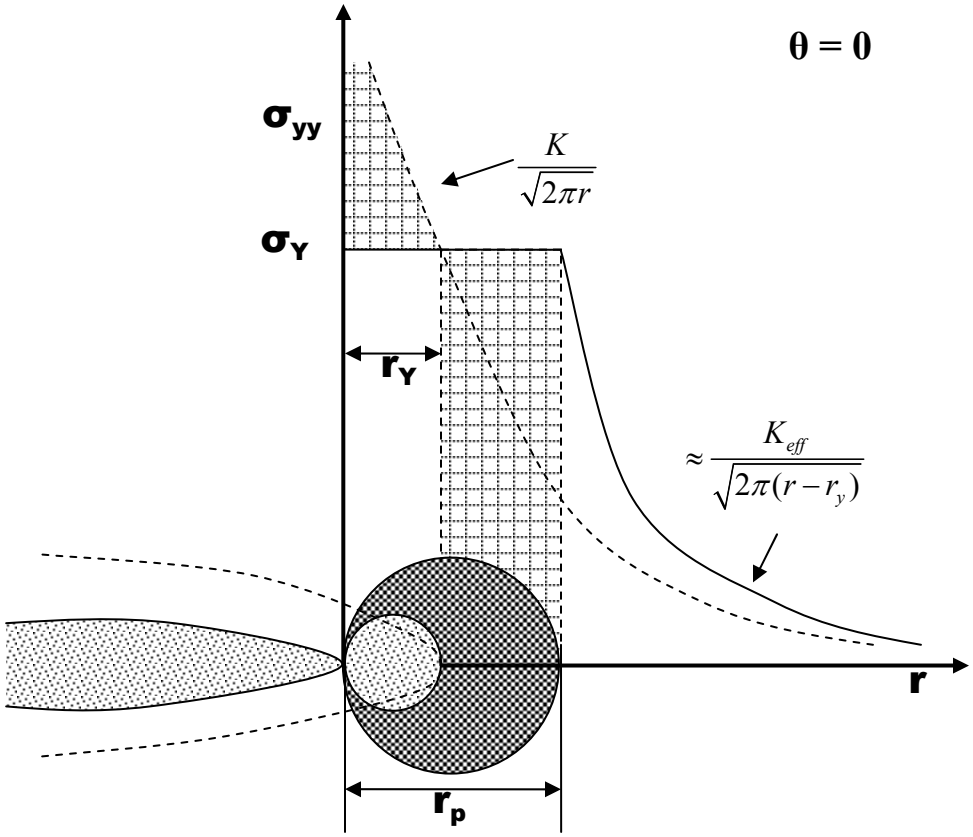

Fig. 2.5 Irwin's elastoplastic stress solution at the crack tip under small scale yielding condition. The broken curve represents the stress solution at the crack tip in linear elasticity, and the solid curve is Irwin's stress solution at the crack tip for linear elastic-perfectly plastic material under small scale yielding condition.

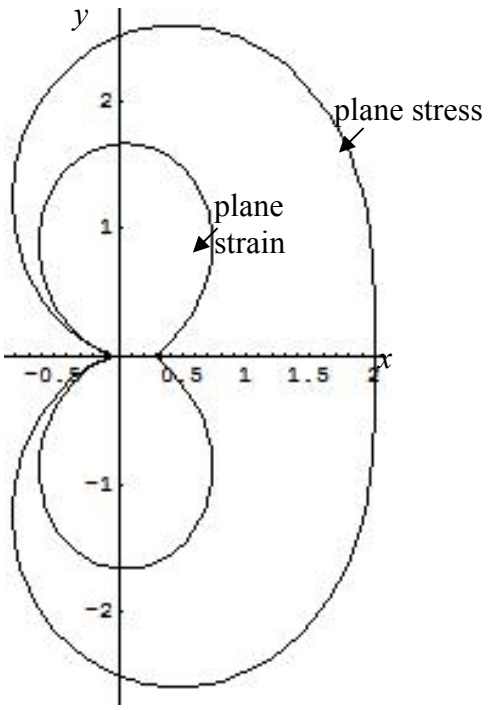

Fig. 2.6 The plastic zone shape at the crack tip under Mode I by von Mises criterion. The crack tip is located at the origin. Crack is located along $-x$ axis. The plot shows the contour of the constant equivalent stress σ_e ($=\sigma_Y$) upon yielding respectively in plane stress and plane strain condition.

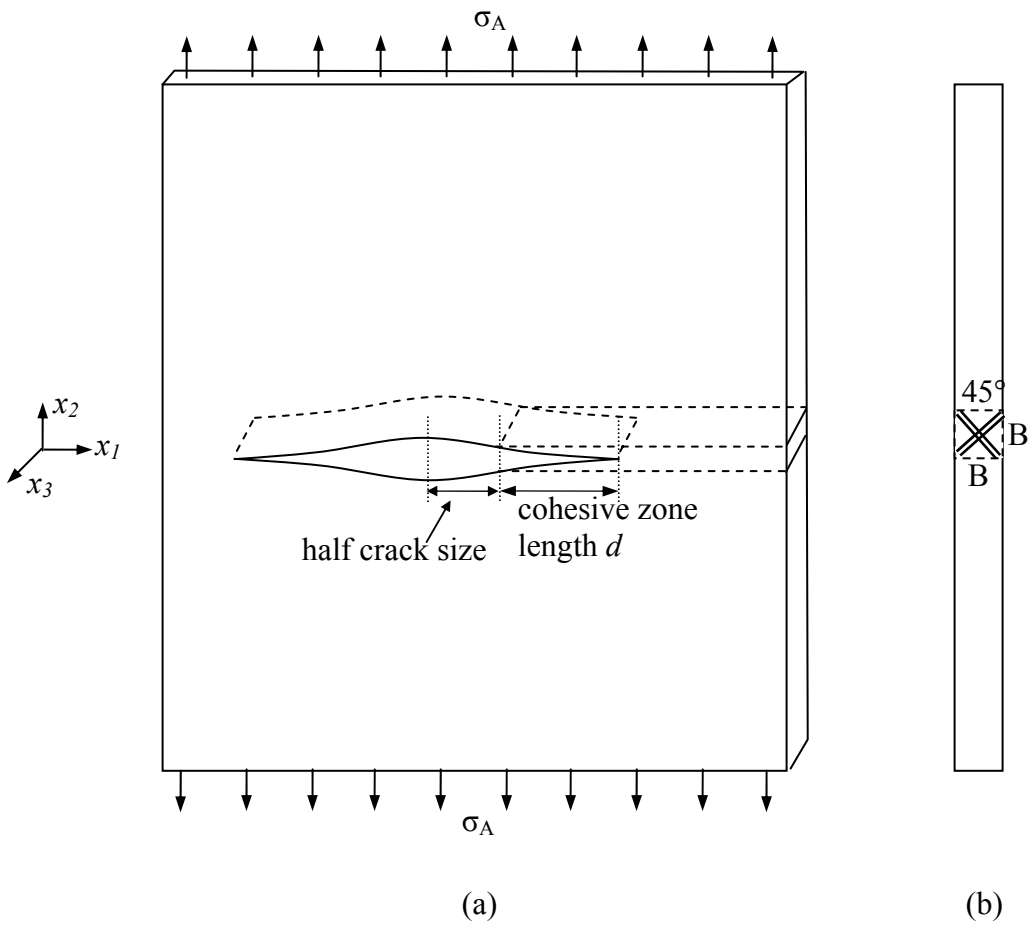

Fig. 2.7 Illustration of Dugdale's Model. A crack resides in a large steel sheet subject to far-field uniform tension. The length of the cohesive zone (a) is *d*, and the height of the cohesive zone (b) is the same as the thickness. The slip lines are 45 degrees to the x_2 and x_3 axes.

CHAPTER 3

THE RELATIONSHIPS BETWEEN WEIGHT FUNCTIONS, GEOMETRIC FUNCTIONS, AND COMPLIANCE FUNCTIONS IN LINEAR ELASTIC FRACTURE MECHANICS

3.1 INTRODUCTION

Linear elastic fracture mechanics (LEFM) employs linear elasticity, a branch of continuum mechanics, to quantify the loading conditions at which an isotropic, linear elastic structure fails due to an extension of a major crack contained in it. Linear elastic fracture mechanics is well-established and has been widely used in industry. As discussed in the last chapter, the stress intensity factor replaces the energy release rate as the macroscopic energy parameter that relates the external loading with the flaw size. Accordingly, an essential element in LEFM is to formulate the expressions for stress intensity factors in terms of external loading and the flaw size. Geometric functions, weight functions, and compliance functions are developed for the above purpose. Geometric functions and weight functions are utilized to obtain the stress intensity factors once the following information is known: flaw size, loading and loading positions, and the geometry of the structure. Compliance functions are employed to determine the crack

length when optical observation is inconvenient. These functions have been intensively studied; nevertheless, the relations between them have received less attention. Therefore, the aim of the work is to investigate the relationships between geometric functions, weight functions and compliance functions in linear elastic fracture mechanics.

A brief introduction is presented in section 3.2 on geometric functions, weight functions and compliance functions in LEFM. The relations between the three functions under mode I are studied in section 3.3, followed by an example on single-edge cracked plate under tension and bending in section 3.4 to illustrate the application of the relations between these functions.

3.2 SPECIAL FUNCTIONS

This work only considers solutions for symmetric specimens under symmetric loading in Mode I with small infinitesimal deformation in a 2-D linear elastic isotropic material. As a result, the following statements hold true: i) The direction of crack propagation is perpendicular to the applied loading under Mode I; ii) The direction of displacement is the same as the loading direction in small infinitesimal displacement case; iii) Field force (body force), such as gravity, electromagnetic field, etc., is not taken account into the derivation; iv) The x-coordinate is taken along crack, i.e., the symmetric line of the specimen, and y-coordinate is in line with loading line, as shown in Fig. 3.1a and 3.1b; and v) The thickness of any specimen is invariant so that the 2-D solution of stress intensity is applicable in 3-D structures.

Consider a symmetric specimen under symmetric loading (Fig. 3.1). The virtual work is formulated by Eq. (2.11):

$$\mathcal{V} = 2Pu_{lp} = 2B\int_{\Gamma} t\,u\,dl, \tag{3.1}$$

where u_{lp} is the load-point displacement, B is the thickness, Γ is one side of the boundary where the traction t is applied, l is the length of Γ, and u is the resulting displacement. Γ is only taken on one side due to symmetry of the stress distribution and the geometry of the specimen. Hence the energy release rate is obtained from Eq. (2.16), i.e.

$$\frac{K_I^{\,2}}{E} = \mathcal{G} = \frac{1}{2}\frac{d\mathcal{V}}{Bda} = \frac{P}{B}\frac{du_{lp}}{da}\bigg|_P = \frac{\int_{\Gamma}(tdu)\,dl}{da}. \tag{3.2}$$

3.2.1 Geometric Function

Stress intensity factors are so far the most successful concept applied in engineering design because researchers developed the expressions of the stress intensity factors in terms of external loading for different geometries:

$$\begin{aligned} K_I &= \sigma_A\sqrt{\pi a}\,Q^*(a/W) = \sigma_A\sqrt{W}\,Q(\alpha) \\ &= \frac{P}{B\sqrt{W}}\,f(a/W) = \frac{P}{B\sqrt{W}}\,f(\alpha), \end{aligned} \tag{3.3}$$

where σ_A is externally applied far-field stress uniform along the width (W) of the specimen, α (= a/W) is the normalized non-dimensional crack length, $Q(\alpha)$ and $f(\alpha)$ are the geometric functions respectively for far-field stress and a pair of concentrated force, and $Q(\alpha) = \sqrt{\pi\alpha}\,Q^*(\alpha)$.

3.2.2 Weight Function

Weight functions are a powerful and cost-effective tool to determine the stress intensity factor and displacement of an isotropic linear-elastic body in presence of complicated loading. It is defined as

$$h_I(\underset{\sim}{x},a)=\frac{E}{2K_I(a)}\frac{\partial u(\underset{\sim}{x},a)}{\partial a}\bigg|_P, \tag{3.4}$$

where $h_I(\underset{\sim}{x},a)$ is the weight function in mode I, and $\underset{\sim}{x}$ is an arbitrary position in the specimen. A non-dimensional form of the weight function, $\tilde{h}_I(\underset{\sim}{x},\alpha)$, is defined as:

$$\tilde{h}_I(\underset{\sim}{x},\alpha)=\sqrt{W}h_I(\underset{\sim}{x},a)=\frac{E}{2K_I(\alpha)\sqrt{W}}\frac{\partial u(\underset{\sim}{x},\alpha)}{\partial \alpha}\bigg|_P. \tag{3.5}$$

The weight function is derived from Betty's theorem [1]. Details of the derivation can be found in Wu's book [2]. Only in symmetric geometry under symmetric loading does the weight function have unique solution[3].

With complicated loading, the stress intensity factor is indeed an integral of the traction and the weight function along the boundary;

$$\begin{aligned}K_I(\alpha)&=2\int_\Gamma t(\underset{\sim}{x})h_I(\underset{\sim}{x},a)d\!\!\!/l\\&=2\sqrt{W}\int_\Gamma t(\underset{\sim}{x})\tilde{h}_I(\underset{\sim}{x},\alpha)d\!\!\!/l,\ \underset{\sim}{x}\in\Gamma.\end{aligned} \tag{3.6}$$

Displacement can also be determined from the weight function by rearranging Eqs. (3.4) and (3.5).

$$u(\underset{\sim}{x},a)=\frac{2}{E}\int_0^a K_I(a')h_I(\underset{\sim}{x},a')d\!\!\!/a'+u_{nc}(\underset{\sim}{x}); \tag{3.7}$$

$$u(\underset{\sim}{x},\alpha)=\frac{2\sqrt{W}}{E}\int_0^\alpha K_I(\alpha')\tilde{h}_I(\underset{\sim}{x},\alpha')d\!\!\!/\alpha'+u_{nc}(\underset{\sim}{x}), \tag{3.8}$$

where $u_{nc}(\underset{\sim}{x})$ is an integral constant at position $\underset{\sim}{x}$, representing the displacement caused by the structure if no crack exists. The meaning of this integral constant will be addressed in detail in section 3.3.4.

3.2.3 Compliance Function

Compliance (C) is the ratio of deformation to load, i.e. the reciprocal of stiffness. Deformation may be displacement or strain; loading may be concentrated force, far-field stress, or bending moment. In this work, compliance is defined as the ratio of *relative* displacement between two symmetric points with respect to loading.

In isotropic linear elastic material, deformation and load has a linear relationship. This enables the compliance as a method to determine the *in-situ* crack length since the compliance value only depends on the ratio, but not specific magnitude of the load. The non-dimensional compliance is expressed as a function of normalized crack length;

$$\begin{aligned} \tilde{C}(\underset{\sim}{x},\alpha) &= \frac{EB2u(\underset{\sim}{x},\alpha)}{P} \\ &= \frac{E2u(\underset{\sim}{x},\alpha)}{\sigma_A W}, \end{aligned} \tag{3.9}$$

where $\tilde{C}(\underset{\sim}{x},\alpha)$ is the non-dimensional compliance function of position $\underset{\sim}{x}$ and crack length.

3.3 RELATIONSHIPS BETWEEN GEOMETRIC FUNCTIONS, WEIGHT FUNCTIONS, AND COMPLIANCE FUNCTIONS

3.3.1 Weight Function and Geometric Function

Consider loading the material with two symmetric-concentrated forces. Combining Eqs. (3.2), (3.3), and (3.5) yields

$$f(\alpha) = 2\tilde{h}_I(lp, \alpha). \tag{3.10}$$

In the case of loading with a far-field uniform stress, the following relation holds:

$$Q(\alpha) = \frac{2\int_\Gamma \tilde{h}(\underset{\sim}{x}, \alpha) dl}{W} = \frac{l}{W} 2\tilde{h}(avg, \alpha), \underset{\sim}{x} \in \Gamma, \tag{3.11}$$

where $\tilde{h}(avg, \alpha)$ is the average weight function along boundary Γ.

Eqs. (3.10) and (3.11) show that the geometric function is indeed the non-dimensional weight function. The factor of 2 represents the symmetry of loading, displacement, and geometry in the specimen. Weight functions are essentially only determined by the geometry of the test piece and the evaluation positions. The geometric function is therefore determined by loading position and the geometry of the structure.

3.3.2 Weight Function and Compliance Function

By combining and rearranging Eqs. (3.3),(3.5) and (3.9), the following is obtained:

$$\begin{aligned} \frac{\partial \tilde{C}(\underset{\sim}{x}, \alpha)}{\partial \alpha} &= 4 f(\alpha) \tilde{h}_I(\underset{\sim}{x}, \alpha) \\ &= 4[\sqrt{\pi\alpha} Q(\alpha)] \tilde{h}_I(\underset{\sim}{x}, \alpha). \end{aligned} \tag{3.12}$$

Eq. (3.12) shows that the compliance function is determined by geometry of the structure, loading positions, the crack size, and the evaluation point.

By integrating Eq. (3.12), the compliance function becomes

$$\begin{aligned}\tilde{C}(\underset{\sim}{x},\alpha) &= \underbrace{\int_0^{\alpha} 4 f(\alpha')\tilde{h}_I(\underset{\sim}{x},\alpha')d\alpha'}_{\text{due to crack}} + \underbrace{\tilde{C}_{nc}(\underset{\sim}{x})}_{\text{no crack}} \\ &= \int_0^{\alpha} 4[\sqrt{\pi\alpha'}Q(\alpha')]\tilde{h}_I(\underset{\sim}{x},\alpha')d\alpha' + \tilde{C}_{nc}(\underset{\sim}{x}),\end{aligned} \tag{3.13}$$

where

$$\begin{aligned}\tilde{C}_{nc}(\underset{\sim}{x}) &= \frac{2EBu_{nc}(\underset{\sim}{x})}{P} \\ &= \frac{2Eu_{nc}(\underset{\sim}{x})}{\sigma_A W}.\end{aligned} \tag{3.14}$$

Eqs. (3.13) and (3.14) can also be derived from (3.8). Eq. (3.13) implies that the compliance of a cracked body is composed of two parts: a constant value part independent of the crack and a varying part due to the presence of the crack. The meaning of the integral constants $u_{nc}(\underset{\sim}{x})$ and $\tilde{C}_{nc}(\underset{\sim}{x})$ will be discussed in 3.3.4.

3.3.3 Geometric Function and the Load-Point Compliance Function

In the case of two symmetric concentrated forces, combining Eqs. (3.10) and (3.12) yields the following relation at the loading point:

$$\frac{\partial\tilde{C}(lp,\alpha)}{\partial\alpha} = 2[f(\alpha)]^2. \tag{3.15}$$

This is a well-known relation between the load-point compliance and the geometric function [4] in case of two symmetric concentrated forces.

3.3.4 Discussion

3.3.4.1 Integral Constants for Displacement Fields and Compliance Functions

Consider the cracked body in Fig. 3.2a. Since superposition holds true for both displacement and stress fields in linear elasticity, the displacement and stress fields for any loaded structure can be viewed as superposition of two bodies: one with stress acting upon crack surfaces and another with concentrated forces applied to the intact body (without crack). When a crack propagates at constant load, the contribution of displacement/compliance due to the intact body remains the constant; whereas the contribution of displacement/compliance due to the crack increases. The displacement contribution from the intact body is calculated with the specific load, loading position and geometry of the structure. However, the compliance of the intact body is only determined by the loading position and geometry of the structure due to the constant compliance in linear elasticity.

One application of Eq. (3.13) is to calculate the crack opening displacement and the crack opening compliance in a symmetric specimen with symmetric loading. In this case, the contribution of displacement/compliance from the uncracked body is zero due to the symmetry, so no integral constants are needed.

3.3.4.2 Comparison of the Special Functions

As shown in Table 3.1, the weight function is unique and ubiquitous in LEFM. It is only a function of the geometry of the structure, which changes in evaluation position and crack length. It is independent of the loading position. The geometric function is, in

essence, a non-dimensional weight function at the loading position. A compliance function is composed of two parts: one part that changes due to crack extension and a constant part from the intact structure which is without any crack. The changing part of the compliance is the integral of a product of weight functions at loading position and the evaluation position, respectively.

3.4 AN EXAMPLE ON SINGLE-EDGE CRACKED PLATE

Single-edge cracked plate (Fig. 3.3a) is a geometry widely employed in fracture and fatigue tests. It is used in either uniform tension (Fig. 3.3b) or bending configuration (Fig. 3.3c). Although the loading position is different in the above two methods, the weight function is the same, independent of loading positions. The weight function at the crack mouth can be determined by the crack-mouth opening displacement (CMOD) compliance function and the geometric function for single-edge cracked plate under uniform tension. Then the CMOD compliance function for bend specimen can be calculated by the weight function and the geometric function for bending configuration since the integral constant is zero in symmetric specimen under symmetric loading.

3.4.1 Uniform Tension

As shown in Fig. 3.3b, the stress intensity factor for single-edge cracked plate under tension is [4]

$$Q(\alpha) = \sqrt{2\tan(\pi\alpha/2)}\,\frac{0.752 + 2.02\alpha + 0.37[1-\sin(\pi\alpha/2)]^3}{\cos(\pi\alpha/2)}. \qquad (3.16)$$

The expression for $Q(\alpha)$ is accurate within ± 0.5% for 0 < α < 1. The CMOD compliance for single-edge cracked plate under tension is [4]:

$$\frac{2Eu(cm,\alpha)}{\sigma_A W} = 4\alpha \frac{1.46 + 3.42(1-\cos(\pi\alpha/2))}{[\cos(\pi\alpha/2)]^2} \tag{3.17}$$

where $u(cm,\alpha)$ is the displacement at the crack mouth. This expression is accurate within ± 1% for 0 < α < 1. With the geometric function and the compliance function known, the weight function at the crack mouth is obtained by Eq. (3.12). The values are compared with Fett's solution [5] (Fig. 3.4):

$$\tilde{h}(cm,\alpha) = \frac{1 + (0.84683 - 0.07567\alpha + 11.7732\alpha^2 - 11.6391\alpha^3 + 4.0684\alpha^4)/(1-\alpha)^{3/2}}{\sqrt{2\pi\alpha}}. \tag{3.18}$$

Fett's solution is accurate within ± 3% for 0 < α <0.85. The discrepancy is within ± 5% between the solutions derived from Eq. (3.12) and provided by Fett.

3.4.2 CMOD Compliance for the 3-Point Bend Specimen

According to ASTM E399, the bending span is four times the width for single-edge cracked plate under 3-point bending (Fig. 3.3c). If the stress intensity factor is expressed in terms of concentrated force, the geometric function is:

$$f(\alpha) = \frac{6\sqrt{\alpha}[1.99 - \alpha(1-\alpha)(2.15 - 3.93\alpha + 2.7\alpha^2)]}{(1+2\alpha)(1-\alpha)^{3/2}} \tag{3.19}$$

This expression for the geometric function is accurate within ± 0.5% for 0<α<1. In this loading configuration, the concentrated force is parallel to the crack; therefore, the geometric function is related to the non-dimensional weight function in mode II.

With the weight function and the geometric function known, the CMOD compliance function for 3-point bend specimen is obtained from Eq. (3.13). The results are compared with the known solution from ASTM E399 (Fig. 3.5):

$$\tilde{C}(cm,\alpha) = 24\alpha(0.76 - 2.28\alpha + 3.87\alpha^2 - 2.04\alpha^3 + \frac{0.66}{(1-\alpha)^2}), \qquad (3.20)$$

which is accurate within ± 1% for 0<α<1. The discrepancy between solutions derived from Eq. (3.13) and provided by ASTM E-399 is within ± 4%.

This example verifies the relations between geometric functions, weight functions and compliance functions in Eqs. (3.12) and (3.13). It shows that any function of the above three functions could be obtained once the other are known and can be used to simplify the numerical process.

3.5 SUMMARY AND CONCLUSIONS

Geometric functions, weight functions, and compliance functions are important in linear elastic fracture mechanics. The following conclusions can be reached.

1. All the three functions are functions of crack length and evaluation point. Particularly, the geometric function is evaluated at loading position, which is in essence the non-dimensional weight function. Eq. (3.15) always holds true whether load is perpendicular or parallel to the crack.

2. Weight functions are only determined by geometry of the specimen, whereas geometric functions and compliance functions are also influenced by loading distribution and position.
3. Displacement/compliance of a cracked body is composed of two parts: changing part due to crack extension and a constant part of the structure if the crack did not exist. In addition, the derivative of compliance with respect to the normalized crack is proportional to the product of the geometric function and the weight function at the evaluation point.
4. The displacement/compliance function at any point can be obtained by Eqs. (3.8) and (3.13) respectively. The integral constant, i.e., the contribution can be solved from the structure if crack did not exist. This will greatly simplify the numerical process in obtaining the displacement/compliance solution using traditional method.

REFERENCES

1. Sokolnikoff, I.S., *Mathematical theory of elasticity*. 2nd ed. 1956: McGraw-Hill Book Company. 476 p.
2. Wu, X.-R. and A.J. Carlsson, *Weight Functions and Stress Intensity Factor Solutions*. 1st ed. 1991: Pergamon Press. 513 p.
3. Rice, J.R., *Some Remarks on Elastic Crack-Tip Stress Fields.* International Journal of Solids and Structure, 1972. **8**: p. p751-758.
4. Tada, H., P.C. Paris, and G.R. Irwin, eds. *The stress analysis of cracks handbook*. 3rd ed. 2000, ASME Press. 677 p.
5. Fett, T. and D. Munz, *Stress Intensity Factors and Weight Functions*. 1st ed. International series on advances in fracture,1366-7114. 1997: Computational Mechanics Publications. 385 p.

Tables and Figures

Table 3.1 Comparison of geometric functions, weight functions and compliance functions.

Dependence	Variables		Determined by	
	Crack size	Evaluation point	Geometry	Loading position & distribution
Weight function	Yes	Yes	Yes	No
Geometric function	Yes	Fixed at loading position	Yes	Yes
Compliance function	Yes	Yes	Yes	Yes

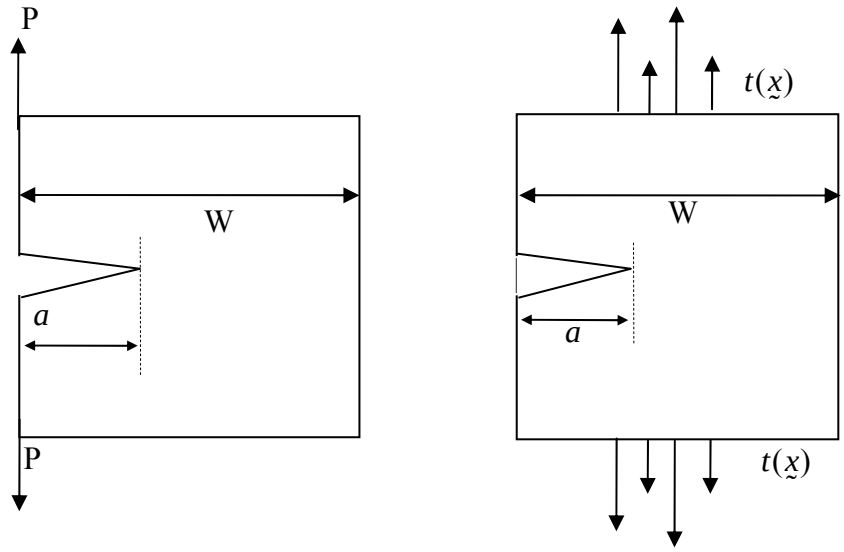

(a) concentrated force (b) stress field on boundary $\partial\Omega$

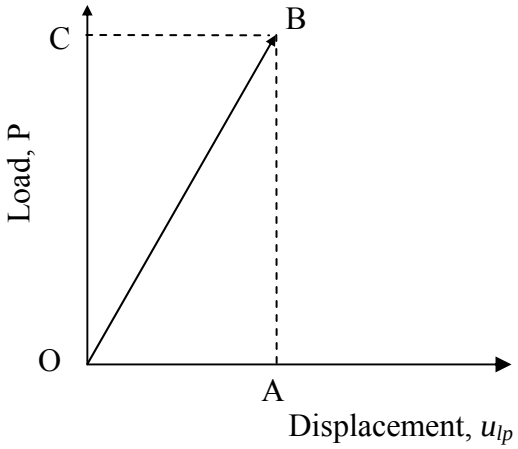

(c) Load-displacement curve. Actual work is area OAB, and virtual work is area OABC.

Fig. 3.1 Symmetric specimen under symmetric loading of either (a) concentrated forces or (b) traction along the boundary. The load-displacement curve shows that the actual work is the area OAB and the virtual work is area OABC in LEFM.

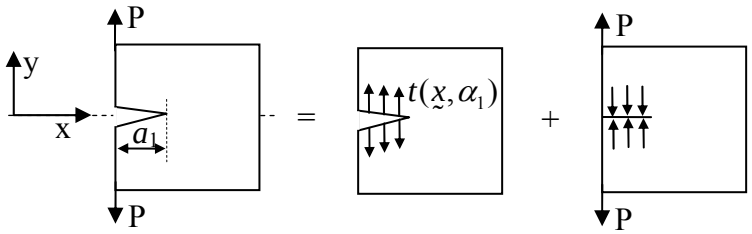

$$
\begin{array}{lcll}
u(\underset{\sim}{x},\alpha_1) & & u^{(A)}(\underset{\sim}{x},\alpha_1) & u_{nc}^{(B)}(\underset{\sim}{x})\big|_P \\
\sigma(\underset{\sim}{x},\alpha_1) & = & \sigma^{(A)}(\underset{\sim}{x},\alpha_1) + & \sigma_{nc}^{(B)}(\underset{\sim}{x})\big|_P \\
K_I(\alpha_1) & & K_I^{(A)}(\alpha_1) & 0
\end{array}
$$

(a)

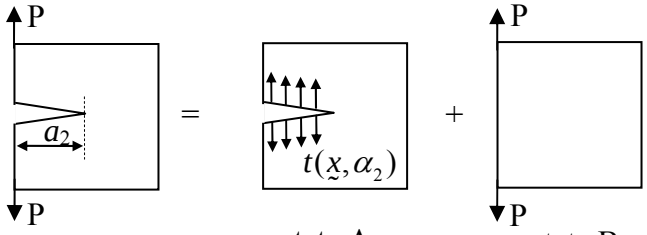

$$
\begin{array}{lcll}
u(\underset{\sim}{x},\alpha_2) & & u^{(A)}(\underset{\sim}{x},\alpha_2) & u_{nc}^{(B)}(\underset{\sim}{x})\big|_P \\
\sigma(\underset{\sim}{x},\alpha_2) & = & \sigma^{(A)}(\underset{\sim}{x},\alpha_2) + & \sigma_{nc}^{(B)}(\underset{\sim}{x})\big|_P \\
K_I(\alpha_2) & & K_I^{(A)}(\alpha_2) & 0
\end{array}
$$

(b)

Fig. 3.2 Schematic plots of linear superposition of displacement field, stress field, and stress intensity factor in an elastic body with different crack length, subjected to a constant load. Obviously, the contribution of displacement, stress, and stress intensity factor are all constant if the external loading is constant during crack propagation.

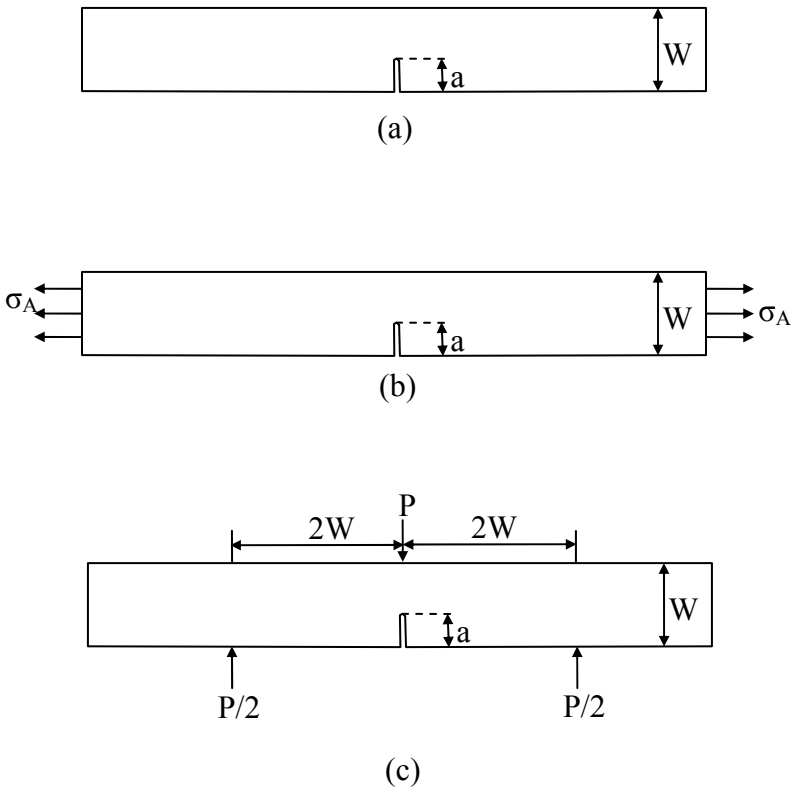

Fig. 3.3 Scheme of single-edge cracked plate (a) loaded under far-field uniform tension (b) and under 3-pt bending (c).

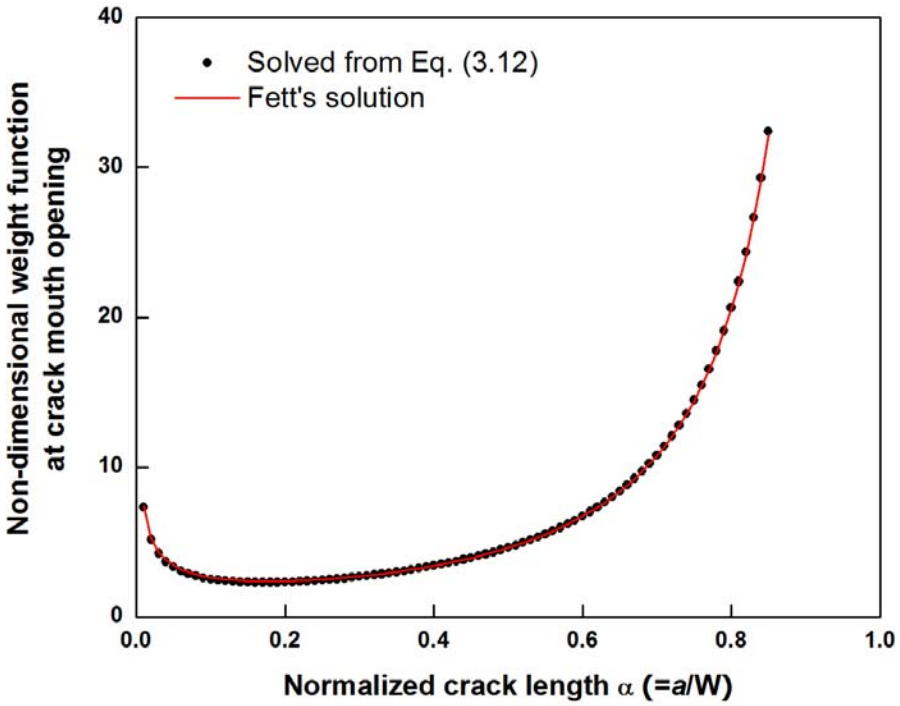

Fig. 3.4 Plot of the non-dimensional weight function of single-edge cracked plate at the crack mouth as a function of normalized crack length α, showing the weight function derived from Eq. (3.12) employing the relation between the geometric function and the CMOD compliance function (solid circles), as compared to Fett's solution [5] (solid line).

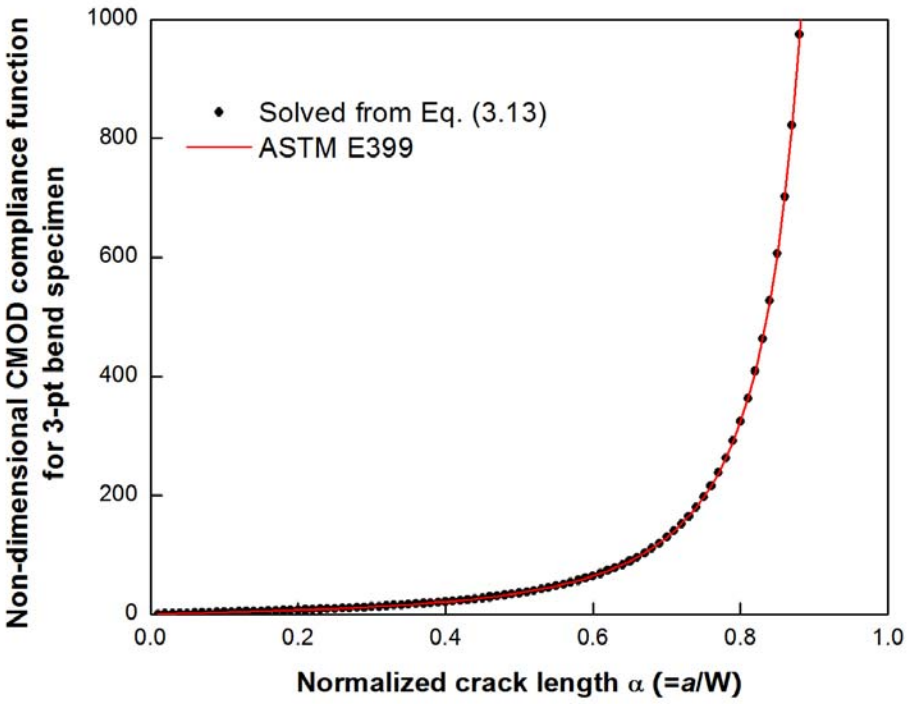

Fig. 3.5 Plot of the non-dimensional CMOD compliance function of 3-pt bend geometry as a function of normalized crack length α, showing the compliance function derived from Eq. (3.13) (solid circles), as compared to the solution according to ASTM E399 (solid line).

CHAPTER 4

ELASTIC COMPLIANCE FUNCTIONS FOR THE NOTCHED FOUR-POINT BEND SPECIMEN

An example is given on single-edged four-point bend (4PB) specimen to illustrate the relationships between geometric functions, weight functions and compliance functions. The compliance functions are numerically determined and experimentally verified respectively for crack-mouth opening displacement compliance, back face strain (BFS) compliance, and load-point displacement (LPD) compliance. With the weight function solutions given by Fett [1] for 4PB geometry, the geometric function is determined independently from the LPD compliance function by Eq. (3.15) and from the CMOD compliance function by Eq. (3.12). The solutions obtained from those two methods show a good agreement, also verifying the conclusions from Chapter 3.

4.1 INTRODUCTION

The single-edge notched four-point bend specimen (SE(B)) is a widely used test geometry in fracture research due to its ease of testing, and the fact that it provides a state of pure bending, i.e., a constant bending moment between the inner two loading points

(minor span).[1] Although not defined in ASTM E 399 standard for fracture toughness testing, geometric functions have been determined for calculating the stress-intensity factor K_I in this specimen geometry as a function of the ratio of the minor span length to the specimen width, d/W [1, 3-5]. Corresponding crack compliance functions for this geometry, however, have received less attention, thereby limiting its use for compliance-based *in situ* crack-length measurements. There are solutions for the crack-mouth opening displacement (CMOD) for pure bending with $d/W = 4$ [4-6], and recently numerically determined and experimentally verified CMOD compliance solutions have been published for $d/W = 2$ [7, 8]. In addition, Huh [9] reported a back-face strain compliance solution for $d/W = 4$.

As there has not been a systematic study of the complete compliance/crack length relationships for the notched four-point bend sample, we present in this note the elastic compliance solutions for this test geometry in terms of the crack-mouth opening displacement, back-face strain compliance, and the load-point displacement, over the range of crack length (a) to width (W) ratios ($\alpha = a/W$) from 0.3 to 0.8. These solutions are applicable to the determination of the fracture toughness and for use with *in situ* monitoring of subcritical crack growth in this test specimen.

[1] This is well utilized in the double-notched version, which is being increasingly used to identify the mechanistic events prior to crack initiation [2]. As both notches experience the same bending moment, when one fractures, the other is "frozen" just prior to fracture and can then be examined metallographically (or otherwise) to identify the "precursor" microstructural events leading to fracture.

4.2 EXPERIMENTS AND SIMULATION

4.2.1 Specimen Geometry and K_I Solutions

To diminish any influence of shear stress resulting from the bending moment outside the minor span (which might cause an underestimate in the energy release rate) and from concentrated stresses at the loading points (which might affect the strain energy field around the notch/crack tip), we examine a four-point SE(B) sample with a large major span where the minor span is at least twice the width [10]. To minimize rotation caused by deviation of the load-point displacements from the load line, we choose the major span to be $4W$ and the minor span to be $2W$ (Fig. 4.1).

The Mode I linear-elastic stress-intensity factor (K_I) for this pure bending geometry is proportional to the remote stress, *i.e.,* the moment, and the geometric factor $Q(\alpha)$, where a is the crack length; it is given for different moment spans with $d/W = 2$ as [6]:

$$\begin{aligned} K_I &= \sigma\sqrt{W}\,Q(\alpha) \\ &= \frac{M}{BW^{3/2}}\,6\,Q(\alpha) \\ &= \frac{P}{BW^{1/2}}\,f(\alpha) \end{aligned} \tag{4.1}$$

and

$$\begin{aligned} Q(\alpha) &= \sqrt{\pi\alpha}\,(2.434 - 20.57\alpha + 78.94\alpha^2 - 127.5\alpha^3 + 80.91\alpha^4) \\ f(\alpha) &= 3Q(\alpha), \end{aligned} \tag{4.2}$$

where $P/2$ is the load applied at each loading point, B is the specimen thickness, M is the bending moment, and $f(\alpha)$ is the geometric function in terms of load. Eq. (4.2) is accurate to within ± 1.0% for $0.2 \le \alpha \le 0.8$ [5].

4.2.2 Experimental Procedures

Two four-point bend specimens were machined from AISI 1080 plain carbon steel to the dimensions indicated in Fig. 4.1. To measure the back-face strain (ε) compliance, a 350 Ω strain gauge, with a 1.57 mm gauge length, was attached to the back face of each specimen, centered along the symmetry line opposite the machined notch. To measure the crack-mouth opening displacement, $2u(cm,\alpha)$, a double-cantilever clip-on displacement gauge (Model 632.02E-20, MTS, Eden Prairie, MN) was placed across the notch mouth.

Cracks were introduced by razor micro-notching and were measured under the optical microscope. At each crack length, the specimen was carefully loaded to minimize local yielding, whereupon measurement of the elastic compliance was made during unloading.

4.2.3 Numerical Methods

Finite-element modeling was performed to ascertain the back-face strain, crack-mouth opening displacement and load-point displacement at 51 values of the normalized crack length, from α = 0.3 to α = 0.8; each value was separated by an increment of α = 0.01. The calculations were performed using the commercial finite-element code ABAQUS, assuming the material was linearly elastic and isotropic with Young's modulus E = 207 GPa, and Poisson's ratio v = 0.3. Plane-strain conditions were assumed for all calculations. The calculations were performed on a mesh with approximately 9,000 degrees of freedom.

4.3 RESULTS AND DISCUSSION

4.3.1 Crack-Mouth Opening Displacement (CMOD)

As noted above, the four-point SE(B) specimen used here is the limiting case of a pure bending geometry. For pure bending specimen, the crack-mouth opening displacement is given by [5]:

$$2u(cm,\alpha) = 4\frac{\sigma W}{E}\alpha V_1(\alpha) = \frac{24M}{EBW}\alpha V_1(\alpha)\,. \tag{4.3}$$

The non-dimensional CMOD compliance function is found by rearranging Eq. (4.3):

$$\frac{EBW\,2u(cm,\alpha)}{M} = 24\alpha V_1(\alpha)\,. \tag{4.4}$$

For d/W = 2, the experimental non-dimensional CMOD compliance results are compared in Fig. 4.2 with our finite-element solutions, as well as the calibration function of Tarafder *et al.* [7]. The numerical solutions are in good agreement with experiment and with the previous solutions [7]. A polynomial fit of the normalized CMOD compliance function is shown in Table 4.1. For application in the direct measurement of crack length, Eq. (4.4) is rearranged to express the normalized crack length, α, as a function of CMOD compliance with the coefficients listed in Table 4.1.

To show the effect of the minor span to width ratio, the numerical CMOD compliance data obtained respectively by Gross[6], Tada[5], and Nisitani[11] for d/W = 4 are included for comparison. It is apparent that the crack-mouth opening displacement for the four-point bend sample increases (at constant bending moment) with the minor span to width ratio; however, the difference is small for $\alpha < 0.4$.

4.3.2 Back-Face Strain (BFS) Compliance

The back-face strain, ε, can be expressed as:

$$\varepsilon = \frac{\sigma}{E} V_2(\alpha) = \frac{6M}{EBW^2} V_2(\alpha). \tag{4.5}$$

Consequently, the non-dimensional BFS compliance function is given by:

$$\frac{EBW^2\varepsilon}{M} = 6V_2(\alpha). \tag{4.6}$$

The experimentally measured and numerically calculated back-face strain compliance is shown in Fig. 4.3 as a function of normalized crack length. The corresponding sixth-degree polynomial-fit function is given in Table 4.2, and describes the experimental results to better than 5% for $0.3 \leq \alpha \leq 0.8$. For use in the direct measurement of crack length, Eq. (4.6) is rearranged to express the normalized crack length as a function of BFS compliance; coefficients are also listed in Table 4.2.

To show the effect of the minor span to width ratio, BFS compliance data from Huh and Song [9] for $d/W = 4$ are included in Fig. 4.3. It is apparent that the back-face strain compliance is independent of the minor span to width-ratio, when d/W ratio is greater than 2.

4.3.3 Load-Point Displacement (LPD)

The non-dimensional load-point displacement, u_{lp}, can be expressed as:

$$\tilde{C}(lp,\alpha) = \frac{EBu_{lp}}{P} = g(\alpha). \tag{4.7}$$

Finite-element calculations of the load-point compliance as a function of normalized

crack length are shown in Fig. 4.4.

Since no experimental data exists, the LPD compliance function obtained by the FEM method is checked indirectly through the geometric function. The geometric function is related to the LPD compliance by Eq. (3.15) [5]:

$$f(\alpha) = \sqrt{\frac{d\tilde{C}(lp,\alpha)}{2\,d\alpha}}\,. \tag{4.8}$$

The geometric function is also independently related to the CMOD compliance by the weight function method:

$$f(\alpha) = \frac{1}{4}\frac{\partial\tilde{C}(cm,\alpha)/\partial\alpha}{\tilde{h}(cm,\alpha)}\,. \tag{4.9}$$

If the LPD compliance is right, the weight function derived from Eq. (4.8) should be the same to that derived from Eq. (4.9). Fig. 4.5 shows the geometric function for the pure bend loading geometry (d/W =2) obtained from the LPD compliance and CMOD compliance respectively. The difference in the geometric function solutions obtained by above two methods is less than 6%, which confirms the validity of the load-point displacement solution.

In order to apply this compliance solution for direct measurements of crack length, listed in Table 4.3 are the corresponding sixth-degree polynomial fit function of the LPD compliance and its inverse function to express the *a/W* as a function of LPD compliance.

4.4 SUMMARY AND CONCLUSIONS

A full set of elastic compliance functions is derived for the single-edge notched four-point (pure) bend SE(B) fracture geometry based on crack-mouth opening displacements, back-face strain compliance and load-point displacements. Good agreement was obtained between experimentally measured and numerically computed solutions for crack lengths varying between 30 and 80% of the sample width ($0.3 \leq a/W \leq 0.8$). Mathematical expressions for the three compliance calibrations are presented for use in the direct measurement of crack length with this test specimen.

REFERENCES

1. T. Fett and D. Munz, *Stress Intensity Factors and Weight Functions*. Billerica, MA 01821, USA: Computational Mechanics Inc. 1997.
2. R.K. Nalla, J.H. Kinney, and R.O. Ritchie, "Mechanistic fracture criteria for the failure of human cortical bone". *Nature Materials*. **2**(3) 2003: p. 164-168.
3. B. Gross and J.E. Srawley, "Stress-Intensity Factors for Single-Edge-Notch Specimens in Bending or Combined Bending and Tension by Boundary Collocation of a Stress Function," *Technical Report NASA TN D-2603*, 1965
4. Y. Murakami, ed. *Stress Intensity Factors Handbook*. 1st ed. Vol. 1. Pergamon Press: Oxford.1986.
5. H. Tada, P.C. Paris, and G.R. Irwin, eds. *The Stress Analysis of Cracks Handbook*. 3rd ed. The American Society of Mechanical Engineers: New York, NY 10016.2000.
6. B. Gross, J. E. Roberts, and J.E. Srawley, "Elastic Displacements for Various Edge-Cracked Plate Specimens". *International Journal of Fracture Mechanics*. **4** 1968: p. 267-276.
7. S. Tarafder, M. Tarader, and V.R. Ranganath, "Compliance Crack Length Relations for the Four-Point Bend Specimen". *Engineering Fracture Mechanics*. **47**(6) 1994: p. 901-907.
8. M. Tarafder, S. Tarafder, and V.R. Ranganath, "Location independent CCL relations for standard fracture mechanics specimens". *International Journal of*

Fatigue. **19**(S8-9) 1997: p. 635-640.

9. Y.-H. Huh and J.-H. Song, "Back-Face Strain Compliance Calibration for the Four-Point Bend Specimen". *KSME International Journal*. **14**(3) 2000: p. 314-319.
10. J.E. Srawley and J. W.F. Brown, eds. *Fracture Toughness Testing Methods*. ASTM STP 381. American Society for Testing and Materials: Chicago, IL.1964.
11. H. Nisitani and K. Mori, "Influence of Supporting Conditions on Stress Intensity Factors for Single-Edge-Cracked Specimens under Bending". *Reports of the Kyushu University*. **58**(5) 1985: p. 751-755.

TABLES AND FIGURES

Table 4.1. Coeffeicients for crack-mouth opening displacement compliance calibration function: $\frac{EBW\delta}{M} = 24\alpha(\beta_0 + \beta_1\alpha + \beta_2\alpha^2 + \beta_3\alpha^3 + \beta_4\alpha^4 + \beta_5\alpha^5)$, and the inverse CMOD compliance calibration function for crack length measurement: $\frac{a}{W} = \beta_0' + \beta_1'U + \beta_2'U^2 + \beta_3'U^3 + \beta_4'U^4 + \beta_5'U^5$, where $U = \frac{1}{\sqrt{EBW\delta / M} + 1}$, for $0.3 \leq a/W \leq 0.8$.

Degree, i	Coefficient, β_i	Coefficient, β'_i
0	-55.76	1.009
1	609.2	-3.853
2	-2552	2.202
3	5279	-0.1630
4	-5380	28.26
5	2189	-43.68

Table 4.2. Coefficients for back-face elastic strain compliance calibration function: $-\frac{EBW^2\varepsilon}{M} = 6(\beta_0 + \beta_1\alpha + \beta_2\alpha^2 + \beta_3\alpha^3 + \beta_4\alpha^4 + \beta_5\alpha^5 + \beta_6\alpha^6)$, and the inverse back-face strain compliance calibration function for crack length measurement: $\frac{a}{W} = \beta_0' + \beta_1' U + \beta_2' U^2 + \beta_3' U^3 + \beta_4' U^4 + \beta_5' U^5 + \beta_6' U^6$, where $U = \frac{1}{\sqrt{-EBW^2\varepsilon / M} + 1}$, for 0.3 $\leq a/W \leq 0.8$.

Degree, i	Coefficient, β_i	Coefficient, β'_i
0	66.022	1.0006
1	-848.39	-1.4396
2	4539.1	-16.221
3	-12727	134.73
4	19838	-723.11
5	-16310	2009.6
6	5568.4	-2318.6

Table 4.3. Coefficients for load-line displacement compliance calibration function: $\frac{EB\Delta}{P} = 6(\beta_0 + \beta_1\alpha + \beta_2\alpha^2 + \beta_3\alpha^3 + \beta_4\alpha^4 + \beta_5\alpha^5 + \beta_6\alpha^6)$, and the inverse CMOD compliance calibration function for crack length measurement: $\frac{a}{W} = \beta_0' + \beta_1' U + \beta_2' U^2 + \beta_3' U^3 + \beta_4' U^4 + \beta_5' U^5 + \beta_6' U^6$, where $U = \frac{1}{\sqrt{EB\Delta / P} + 1}$, for $0.3 \leq a/W \leq 0.8$.

Degree, i	Coefficient, β_i	Coefficient, β'_i
0	61.962	-0.057
1	-782.93	45.024
2	4181.6	-853.75
3	-11709	8155.7
4	18217	-43643
5	-14945	123443
6	5086.5	-145492

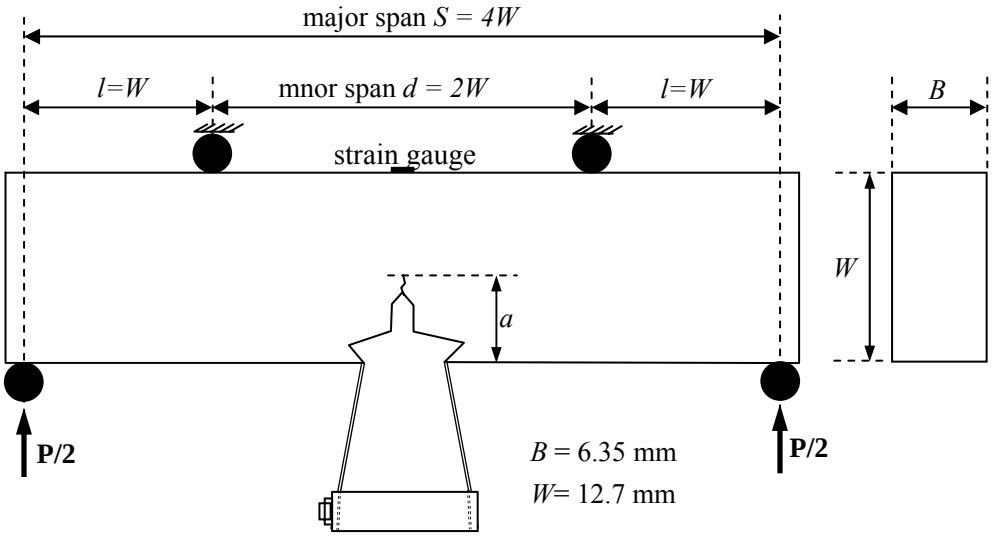

Fig. 4.1. Four-point bending specimen with major span (*S*) to width (*W*) of 4, and minor span (*d*) to width ratio of 2. The moment span is (*S*-*W*)/2, and *B* is the thickness. A strain gage is placed on the center of the back face and a double cantilever clip-in displacement gage is placed across the crack mouth. The details of the crack-mouth geometry can be seen in ASTM E 399.

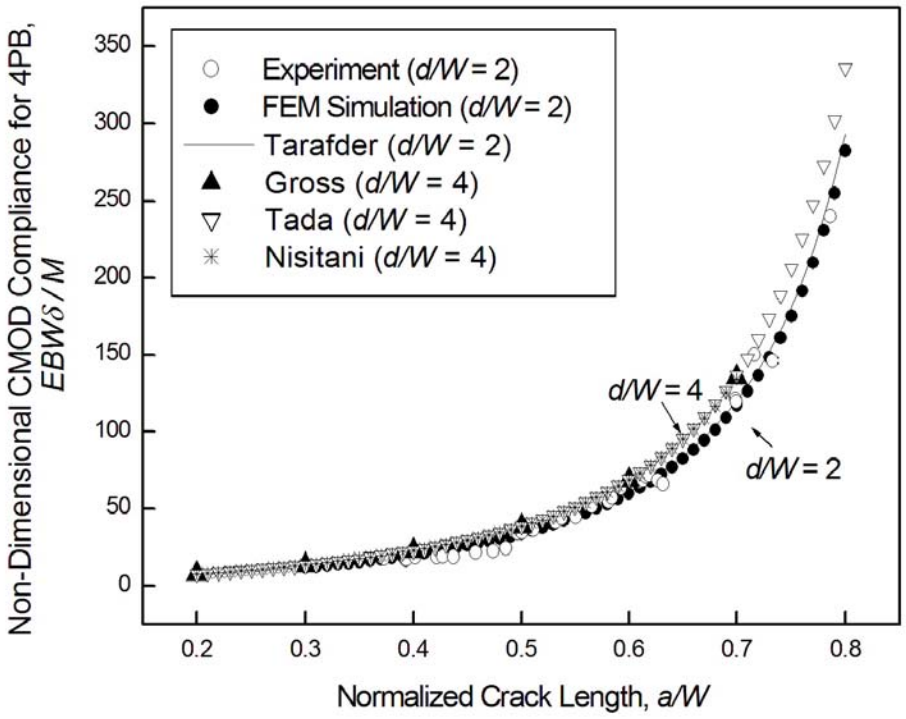

Fig. 4.2. Plot of the crack-mouth opening displacement compliance calibration, as a function of crack length, for the single-edge notched four-point bend specimen ($d/W = 2$) showing both the experimental data (open circles) and the numerical solution (filled circles), as compared to Tarafder *et al.*'s finite-element solution (solid line) [7]. The numerical compliance calibration for $d/W = 4$ is included for comparison [5, 6, 11].

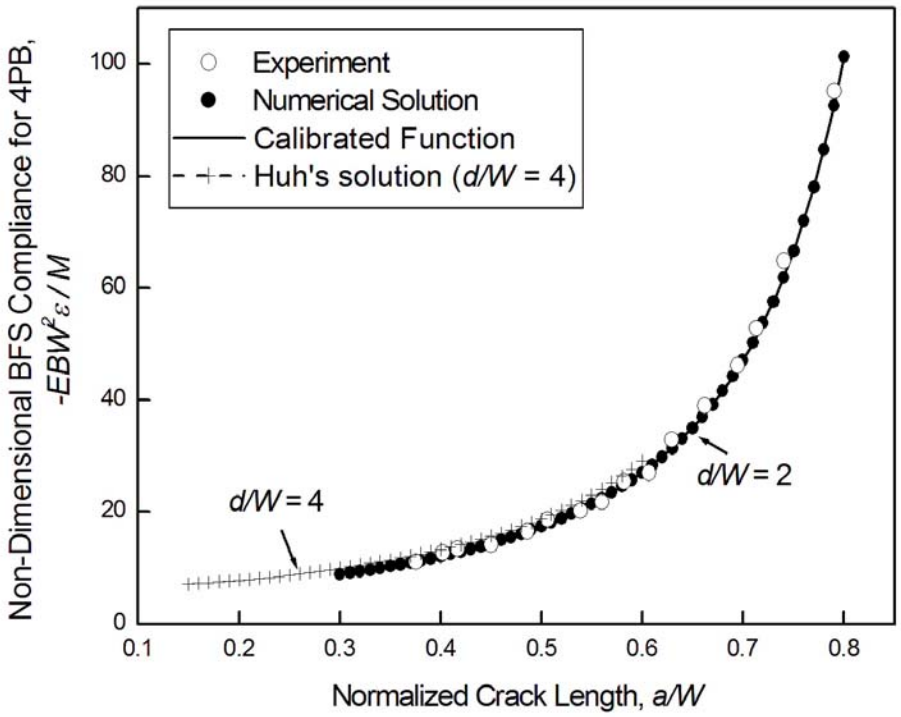

Fig. 4.3. Plot of the back-face strain compliance calibration, as a function of crack length, for the single-edge notched four-point bend specimen ($d/W = 2$) showing both the experimental data (open circles) and the numerical solution (filled circles), along with the polynomial fit function (solid line). The numerical and experimental compliance calibration for $d/W = 4$ is included for comparison [9].

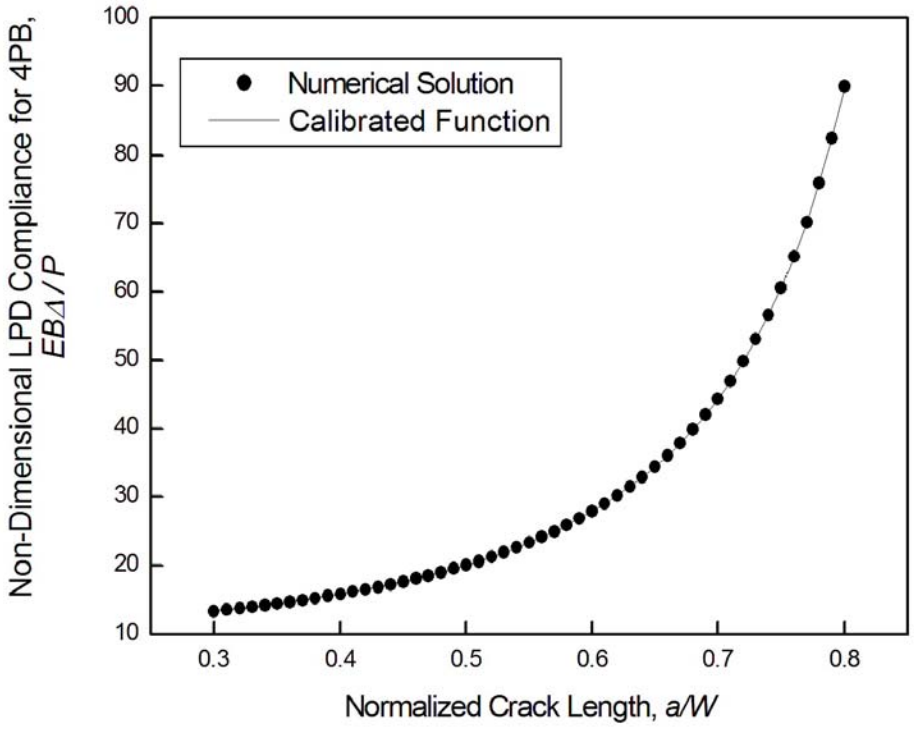

Fig. 4.4. Plot of the 4PB ($d/W = 2$) load-point displacement compliance calibration, as a function of crack length, for the single-edge notched four-point bend specimen ($d/W = 2$) showing both the numerical solution (filled circles) and the polynomial-fit function (solid line).

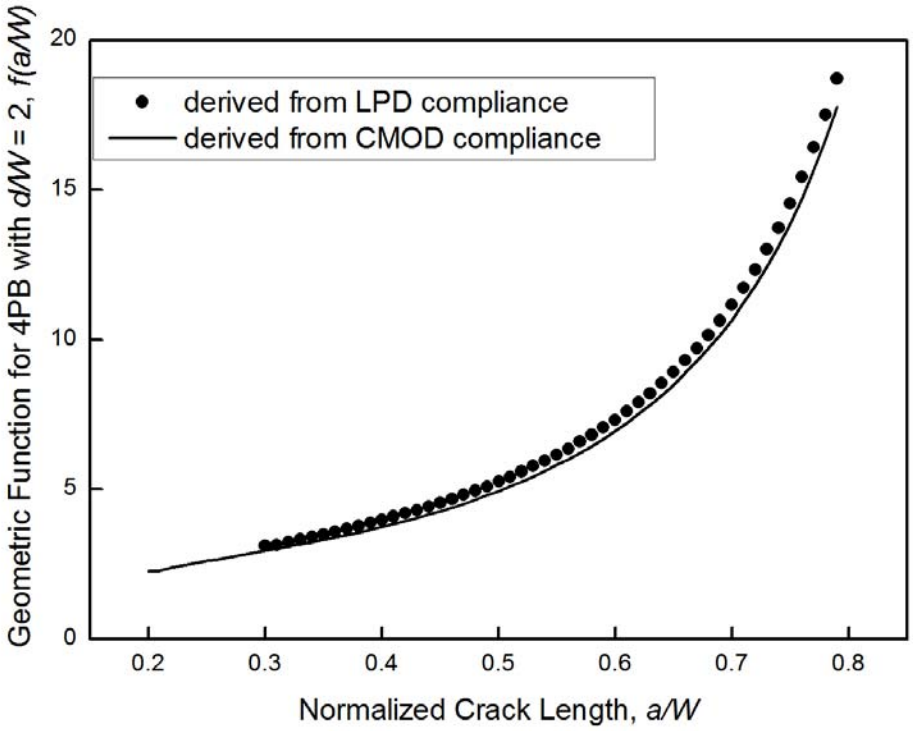

Fig. 4.5. The geometric function for calculating the linear-elastic stress-intensity factor for the single-edge notched four-point bend specimen with the minor span to width ratio of $d/W = 2$. The solid line represents the solution derived from CMOD compliance by Eq. (4.9), and the filled circles represent the solution derived from the load-point displacement solutions computed in this study.

CHAPTER 5

CONCLUSIONS

The relationships between geometric functions, weight functions, and compliance functions were investigated in linear elastic fracture mechanics. The relationships were verifies by examples on single-edge cracked plate under tension and bending. The following conclusions can be reached:

1. The weight function is the most fundamental function in linear elastic fracture mechanics. It is only determined by the geometry of the structure, independent of the loading or loading distribution. The geometric function is essentially the non-dimensional weight function at the loading point. The compliance function is composed of two parts: a varying part due to crack extension and a constant part from the intact structure if no crack exists. The changing part of the compliance function reflects the collaborative deformation response from the loading position and the evaluation point due to crack propagation. Therefore, both the compliance function and the geometric function depend on the geometry of the specimen and the loading positions.
2. The derivative of the load-point compliance function with respect to crack extension is always twice the square of the geometric function in LEFM.
3. Any of the three functions can be obtained once the other two are known. The compliance function is acquired from the integration of the product of the geometric function and the weight function at the evaluation point with respect to the crack size. The integral constant is the unchanging compliance from the

structure if no crack existed. A special application of this integration is to develop the compliance functions along the crack since the integral constant is zero along the crack for symmetric specimens under symmetric loading.

With respect to the future work, methods should be developed for obtaining compliance values of the intact structure without crack for different geometries. Also a review should be carried out on geometric functions, weight functions, and compliance functions for the frequently used test geometries.

The study on the relationships between geometric functions, weight functions, and compliance functions reveals not only the intrinsic relations between these functions, but also the dependence of each function on the testing conditions (the geometry of the structure, the loading positions, etc.). These relations may greatly simplify the numerical process in obtaining either geometric functions, weight functions or compliance functions for new test geometries.